Review article

Simone Ferrari, Carsten Schuck and Wolfram Pernice*

Waveguide-integrated superconducting nanowire single-photon detectors

https://doi.org/10.1515/nanoph-2018-0059
Received May 14, 2018; revised July 31, 2018; accepted August 14, 2018

Abstract: Integration of superconducting nanowire single-photon detectors with nanophotonic waveguides is a key technological step that enables a broad range of classical and quantum technologies on chip-scale platforms. The excellent detection efficiency, timing and noise performance of these detectors have sparked growing interest over the last decade and have found use in diverse applications. Almost 10 years after the first waveguide-coupled superconducting detectors were proposed, here, we review the performance metrics of these devices, compare both superconducting and dielectric waveguide material systems and present prominent emerging applications.

Keywords: integrated optics; single photon detection; superconducting devices.

1 Introduction

The development of reliable micro- and nanofabrication technology has led to compact and low-loss photonic integrated circuits that outperform many bulk optic systems in terms of complexity as well as stability [1–3]. Free-space optical assemblies allow for easy interchange of components compared with integrated systems but suffer from higher optical losses, misalignment, thermal instability and coupling losses to stand-alone sources and detectors. In order to avoid these issues, the integration of optical components for the generation, routing and detection of light is therefore a special requirement for the advancement of quantum optics [4–7]. Within such full assemblies, additional requirements arise for single-photon detectors to provide unitary detection efficiency, no dark counts, zero dead time and vanishing timing uncertainty [8]. Real detectors, however, will only approximate these performance characteristics due to intrinsic limitations of the underlying detection mechanism as well as device imperfections. Often, detectors only perform well for particular characteristics, requiring the experimentalist to trade off one performance benchmark for another. Among the various technologies that have been employed for single-photon detection to date, photo-multiplier tubes (PMTs) [9], semiconducting solid-state devices such as single-photon avalanche diodes (SPADs) [10, 11], visible-light photon counters (VLPCs) [12] and superconducting detectors [13] are particularly widespread. In the class of superconducting detector technologies, transition edge sensors (TES) [14] and superconducting nanowire single-photon detectors (SNSPDs) [15] represent the most attractive devices.

SNSPDs consist of an electrically and optically accessible, very narrow (~100 nm) and ultrathin (4–5 nm) superconducting wire strip, as depicted in Figure 1A, which is easier to integrate when compared with, for instance, semiconductor detectors. The working mechanism of SNSPDs is based on the suppression of the superconducting state upon the absorption of a photon, which is transduced into a detectable electrical signal [17, 18]. Although significant experimental effort has been dedicated to the characterization of SNSPDs [19–28], on a microscopic level, the detection mechanism is not yet fully understood. A shared interpretation in the community runs as follows [17]: when the detector is biased below the depairing current, the absorption of a photon, which has a high energy in comparison to the superconducting energy gap, generates a cloud of quasiparticles (i.e. broken Cooper pairs), resulting in local weakening or suppression of the superconducting state (hot-spot) [29]. Different models have been proposed to explain hot-spot formation and its dynamics. In the earliest model, the so-called *normal core hot-spot*

***Corresponding author: Wolfram Pernice,** University of Münster, Institute of Physics, Münster 48149, Germany; University of Münster, Center for Nanotechnology (CeNTech), Münster 48149, Germany; and University of Münster, Münster Nanofabrication Facility (MNF), Münster 48149, Germany,
e-mail: wolfram.pernice@uni-muenster.de
Simone Ferrari and Carsten Schuck: University of Münster, Institute of Physics, Münster 48149, Germany; University of Münster, Center for Nanotechnology (CeNTech), Münster 48149, Germany; and University of Münster, Münster Nanofabrication Facility (MNF), Münster 48149, Germany

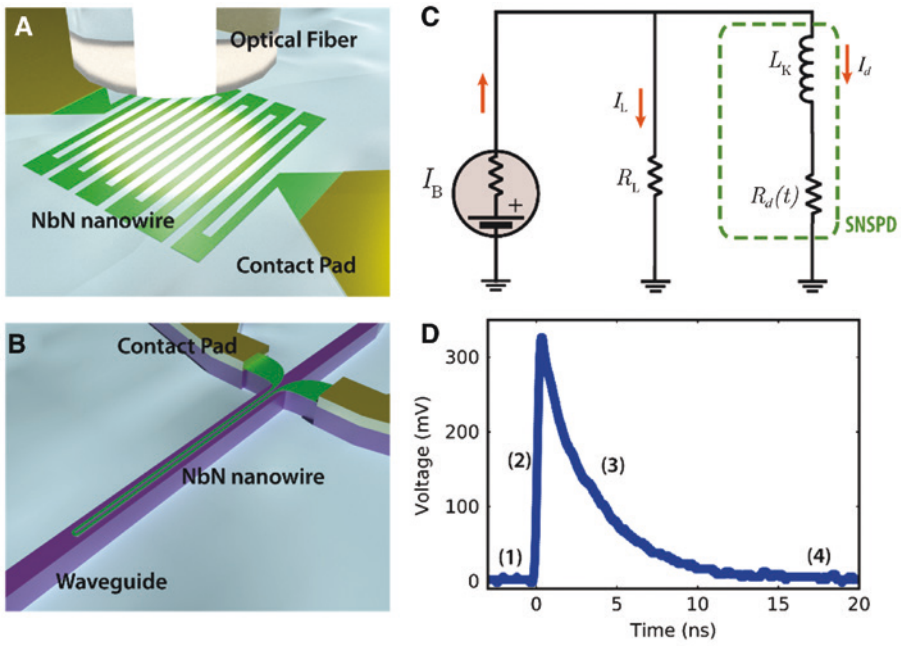

Figure 1: Function of superconducting single photon detectors.
(A) Fiber coupled SNSPD. (B) Waveguide integrated SNSPD. (C) Electrical equivalent circuit of an SNSPD. The nanowire can be described as an LR circuit, where L_K is the kinetic inductance and R_d is the nanowire resistance. R_L is the load resistance, typically equal to 50 Ω. (D) Measured output voltage of an SNSPD. In the superconducting state, all the current flows onto the nanowire with almost no energy dissipation (1). After the absorption of a photon, the nanowire resistance increased to $R_d >> R_L$; therefore, the current will start flowing onto the load resistance R_L, allowing to obtain a measurable output voltage signal (2). The carrier recombination occurs at a very fast timescale (typically tenth of picosecond for NbN [16]) and the superconducting state is recovered after a transient time, which depends on the carrier inertia and therefore on the kinetic inductance L_K (3). After this time, the biasing condition is fully recovered, and the detector is ready to detect another photon with the original efficiency (4).

model [30–33], the hot-spot is a normal domain inside the superconductor that the bias current should bypass. The transition of the nanowire to the normal resistance state is due to current crowding along this resistive hot-spot and can occur only if the current density around the normal core overcomes the switching current of the device, i.e. the threshold current at which the superconducting nanowire switches to the normal state. As an alternative to this model, diffusion of quasiparticles from the absorption site along the nanowire section has been considered [34]. A hot-belt is generated, forcing the drift velocity of the supercurrent to increase. Switching to the resistive state occurs when the drift velocity overcomes the critical drift velocity of the superconducting carriers. Although these interpretations initially guided the technological development of SNSPDs, these models were purely deterministic and can be adopted for interpreting the detection at high-bias currents and high-energy photons (deterministic region). At low-bias currents and for low-energy photons, instead, current crowding might not be sufficient to switch the nanowire to the normal state (probabilistic region). For this reason, probabilistic processes such as vortex- or vortex-antivortex-pair unbinding and dissipative diffusion away from the quasiparticles nonequilibrium region have been introduced [35–39]. Vortex unbinding can happen also in a region of partially suppressed superconductivity, allowing to abandon the requirement for a normal core or belt but including probabilistic phenomena such as fluctuations of the order parameter [40]. On a macroscopic level, instead, an electrical equivalent model was proposed [21, 41, 42] and was presented in Figure 1C, D. In this model, the detector can be described as a series RL circuit [41], where R_d is the variable nanowire resistance and L_K represents the nanowire kinetic inductance, i.e. the inertia of carriers in the superconducting wire [43].

Since their first realization in 2001 [30], SNSPDs have been developed into one of the most promising technologies for broadband optical detection of single photons. SNSPDs provide superior performance for broadband detection of weak light with high detection efficiency (DE), excellent signal-to-noise ratio (SNR), fast recovery time and low timing uncertainty [8, 15, 44, 45]. The remarkable properties of SNSPDs are beneficial for a broad range of applications in both quantum and classical domains, from quantum computation [46–51], secure communication [52–58] and metrology [59–65] to classical faint light

applications such as fluorescence lifetime imaging microscopy (FLIM) [66, 67], fluorescence correlation spectroscopy (FLCS) [68], fluorescence resonance energy transfer (FRET) [69], single molecule detection [70], time-resolved photoluminescence (TRPL) [71–73], optical time domain reflectometry (OTDR) [74–76] and remote sensing (LiDAR) [77, 78].

Different approaches have been proposed to improve the optical interface to the detector [44]. The easiest approach consists in free-space coupling through focusing optical assemblies. Alternatively, direct coupling with an optical fiber or through fiber-coupled small gradient index focusing lenses with a similar size as the fiber core diameter can be adopted. In these configurations, photons impinge on the detector under normal incidence. The absorption occurs only in the few-nanometer-thick superconducting material; therefore, technological efforts to improve the absorbance of these detectors, including embedding the nanowire in optical cavities [79], as well as detector geometry optimizations to make it insensitive to the polarization of the incident light [80, 81], have been made, allowing to achieve record system detection efficiencies above 90% at infrared wavelengths [82, 83].

A comparison between the different bulk technologies is reported in Table 1. PMTs and SPADs show high detection efficiency in the ultraviolet (UV) to visible (VIS) wavelength range, close to room temperature. To extend their operation to near-infrared (NIR), up-conversion devices exploiting nonlinear processes can be used to convert low-energy photons into the UV-VIS range, with maximal system detection efficiencies of 46% [95]. At NIR wavelengths, InGaAs-based semiconductor detectors achieve the highest sensitivity with modest cooling below room temperature and are the detection technology of choice for many telecom applications. InGaAs APDs, however, are plagued by high dark count rates, poor timing performance and the presence of afterpulses, which limit their application to measurements in gated mode [96]. Superconducting detectors stand out from all detector technologies considered above as they offer superior detection efficiency, higher timing accuracy and lower noise in free running operation over an optical bandwidth spanning the UV to mid-IR wavelength range. These highly attractive performance characteristics are, however, only achieved at cryogenic temperatures below 4.2 K in current devices. This is especially true for TES, where temperatures well below 1 K are mandatory. Despite the corresponding complexity and higher cost of the required cryogenic environment, transition edge sensors are one of the few detector technologies that allow for true photon number resolution (PNR), although this attractive capability comes at the cost of longer device recovery times and larger timing uncertainty.

Stand-alone SNSPDs are ideal for all fiber and free-space applications, but they would lead to coupling losses whenever they need to be interfaced with on-chip devices. Furthermore, to achieve high detection efficiency, these structures must be relatively long and dense meanders are needed (typically covering >200 μm^2 [82]), compromising the speed of the detector and making the devices

Table 1: Performances comparison for stand-alone detector technologies.

	Timing jitter (FWHM)	Dark counts	Maximum count rate	Optical range	DE	PNR	Operating temp.
"Detect" program [84]	<100 fs	<1/day	>10 Gcps	≥3 of X-ray, UV, VIS, IR, MWIR, LWIR simultaneously	>99.9%	$>1–10^3$	300 K
GaAsP PMT [9, 85]	80 ps	<10 kcps	10 Mcps	VIS	40%	Only using spatial/ time multiplexing	300 K
InP/InGaAs PMT [86]	400 ps (TTS)	250 kcps	n.a.	NIR	2%	Intrinsically limited [87]	213 K
VLPC [88]	2 ns [89]	20 kcps	100 kcps	VIS	88%	Intrinsically limited [89]	6.9 K
Si SPAD [90]	20 ps	<100 cps	1 Mcps	VIS	55%	Only using spatial/ time multiplexing	120 K
InGaAs SPAD [91]	140 ps	12 kcps	197 Mcps [92]	NIR	45%	Only using spatial/ time multiplexing	200 K
TES [13, 93]	25 ns	Negligible	1 Mcps	VIS to MIR	>97%	Yes	100 mK
SNSPD [82]	<5 ps [94]	<10 cps	25 Mcps	UV to MIR [19]	>90%	Only using spatial/ time multiplexing	<4 K

The "Detect" program (first row) of the Defense Advanced Research Projects Agency (DARPA) serves as a reference for assessing the fundamental limits of single-photon detector performance [84]. See main text for abbreviations.

more prone to fabrication imperfections [97–99]. Although for applications in quantum information Science and for the detection of faint light, integration of single-photon detectors with on-chip photonic structures represents, in general, a challenging task, thanks to their relatively simple structure, SNSPDs are less demanding. A new approach where detectors are integrated with the experiment directly on the respective chip has been proposed in 2009 by Hu et al. [100]. In this new configuration, a single nanowire segment is placed on top of a photonic waveguide such that photons are absorbed along their direction of propagation, as depicted in Figure 1B. This approach allows for drastically enhancing the interaction length over which the propagating field can be absorbed by the nanowire. Wires of significantly shorter overall length than those of meander-type detectors can then be used to efficiently absorb photons travelling on a chip. Such short wires possess a smaller kinetic inductance and therefore feature smaller recovery times, resulting in higher photon counting rates. In 2011, Sprengers et al. [101] presented the first experimental realization of a superconducting nanowire single-photon detector consisting of an NbN nanowire fabricated on top of a GaAs waveguide. The on-chip detection efficiency (OCDE) was determined as 19.7%, and a timing jitter of 60 ps was measured. Subsequently, Pernice et al. [102] demonstrated NbN superconducting nanowire single-photon detectors embedded with silicon (Si) waveguides featuring 91% OCDE, sub-nanosecond decay time and 18-ps timing jitter in the NIR range. The combination of SNSPDs and nanophotonic represents an added value for performances tunability. The absorption of the detector can be in fact engineered by controlling the evanescent coupling trough waveguide and detector geometry [103], and state-of-the-art nanophotonic structures can be exploited to improve or add new functionalities to the detector, such as high efficiency and spectral resolution by embedding them in microring resonators [104], wavelengths demultiplexer [105] or photonic crystal cavities [106]. In addition, travelling wave geometry evanescent coupling could play an important role in the mitigation of artifacts due to the position dependency of the detection efficiency. It has been in fact observed [102] from mode simulation that, for evanescent coupling, the optical field is concentrated in the side of the nanowire, resulting in a higher absorption efficiency than in the nanowire center. This could have important consequences in the detection mechanism and in the detector performances of the geometrical jitter, for instance, as discussed in the next section.

In Section 2, we gave an overview of the key performance parameters of waveguide-integrated superconducting detectors and compared them with alternative integrated detectors. In Section 3, a review of the most attractive integrated platforms and an overview of the most promising superconducting material systems for waveguide-integrated SNSPDs were presented. In Section 4, we summarized some of the recent achievements in engineering the detector geometry to enhance their performance, in particular, regarding absorption efficiency, PNR and spectral sensitivity. In Sections 5 and 6, we discussed the integration of SNSPDs with nanophotonic circuits for the characterization of the quantum light sources and quantum interference, respectively. In Section 7, we discussed one of the most recent applications of integrated SNSPDs for the implementation of artificial neural networks. This review was concluded in Section 8 with a brief outlook of the open challenges and opportunities for the application of waveguide-integrated SNSPDs.

2 Detector performance characteristics

The crucial performance parameters for single-photon detectors are their detection efficiency, dark count rate, afterpulsing probability, recovery time, jitter, optical bandwidth and photon-number resolving capability [45]. In the following, we assessed each of these characteristics for the case of superconducting nanowire single-photon detectors and further discussed their fabrication yield as well as scaling properties in comparison with other detector technologies.

2.1 Detection efficiency

Detection efficiency is defined as the probability of electronically registering an event upon the arrival of a photon at the detector [45]. System detection efficiency is the product of three main contributions: coupling efficiency, absorption efficiency and internal quantum efficiency. Coupling efficiency considers all the coupling losses from the experiment's optical output channel to the nanowire detector. Absorption efficiency describes the probability that a photon reaching the detector is actually absorbed in the superconducting nanowire material. Internal quantum efficiency is the probability that an absorbed photon is converted into a recordable electrical signal [20]. Superconducting nanowires only realize high detection efficiency if several conditions are satisfied. First, a proper optimization of the optical waveguide-to-nanowire coupling is fundamental to achieve high absorption efficiency, as discussed

in Section 4.1. In addition, it is desirable to operate the device in the deterministic current-crowding regime, where the internal quantum efficiency saturates at its maximum value. Current-crowding detection is predominant in the presence of a large hot-spot radius in comparison with the nanowire width, as observed for small band-gap and long relaxation time superconductors [107] and for high depairing currents [32]. This can be achieved by working well below the critical temperature [108, 109] and by improving the superconducting film quality [110]. The latter aspect becomes more relevant also considering that, to observe current-crowding detection in the presence of a small hot-spot, narrow nanowires will be fabricated [111, 112]. Here inhomogeneities and defects limit the experimentally achievable switching current [113]. In Figure 2A, the characteristic bias current dependence of the OCDE is shown for a silicon nitride (SiN) waveguide-integrated niobium nitride (NbN) SNSPD. The measured detection efficiency saturates close to the critical current, indicating that the detector is operating in the deterministic detection regime. Saturation of the detection efficiency is a desirable feature because it allows for operating the detector in a regime in which small fluctuation of the bias current will hardly affect the detector response. Saturated detection efficiency at low bias currents allows for obtaining a high SNR of the detection system, as discussed in Section 2.2.

For typical stand-alone SNSPDs, system detection efficiency is the relevant parameter of interest, because these devices usually interface with the experiment via fiber or free-space links. In nanophotonic applications, where all the relevant photons are propagating optical waveguides, one often defines the OCDE, which does not consider the insertion losses of external light sources onto the chip. As most material systems that are employed for optical waveguides provide extremely low-loss interfaces between the detector region and the photonic integrated circuitry, which is realized in the experiment under study, only the absorption and internal quantum efficiencies contribute to the OCDE in a meaningful way [102]. The most common method to determine the efficiency of single photon detectors uses carefully calibrated light sources that emit a well-characterized number of photons [45, 114]. In this technique, calibration devices on the chip under test allow for determining the absolute number of incident photons that reach the nanowire detector by monitoring the transmission through a reference port of the device [105, 115]. A calibrated power meter [116] or an integrating sphere is used for precise optical power measurements, and separately calibrated attenuators [117] allow for determining the absolute number of photons reaching the detector. Alternative methods such as the correlated photon method [45, 118, 119] or calibration with synchrotron radiation [120] have also been adopted. The former can suffer from low photon conversion efficiency of the source, while the latter requires access to a suitable synchrotron radiation source, which is not readily available at most laboratories.

2.2 Dark count rate

Single-photon detectors occasionally register events even when none of the sought-after signal photons were incidental [17, 45]. Such detector noise is commonly referred to in terms of the dark count rate, which is made up of three main contributions [111]: electrical noise, background

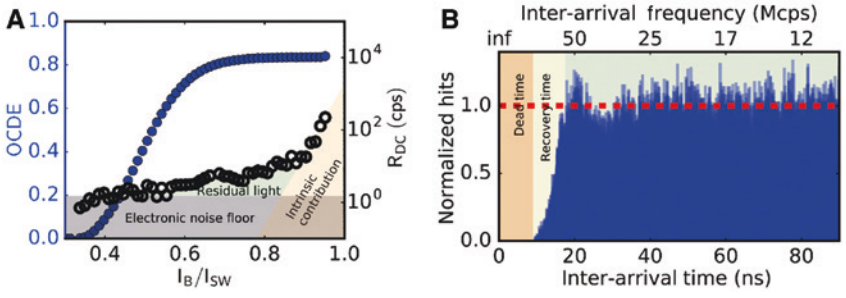

Figure 2: Noise performance of SNSPDs.
(A) In blue (linear scale on the left) is reported the OCDE curve for an NbN SNSPD integrated on a SiN waveguide at different bias currents I_B. The x axis is normalized to the switching current I_{SW}. The efficiency is bias current dependent and reaches a saturation at 80% I_{SW}. In black (log scale on the right) is reported the bias current dependence of the dark count rate. At low bias, the electronic noise floor represents the main contribution, while near I_{SW}, intrinsic dark counts are predominant. In the intermediate range (green shaded area), it is possible to observe the contribution of stray light inside the cryostat sample chamber. (B) Inter-arrival time measurement of a waveguide-integrated SNSPD. For this detector, the dead time, i.t., the time after the detection event in which no other events are recorded is 10 ns, while the overall recovery time (time needed for the detector to recover full efficiency), starting from t = 0, is 18 ns.

radiation and intrinsic dark counts, as depicted in Figure 2A. Electrical noise in the bias and readout circuitry can generate electrical pulses that will inadvertently be interpreted as photon absorption events. The presence of scattered or background light, e.g. blackbody radiation, in the vicinity of the nanowire detector can also lead to undesired detection events, which are unrelated to the optical signal under study. Thermal excitations in a nanowire that is biased close to its critical current can trigger switching from the superconducting to the normal state, thus resulting in electrical output pulses [38, 121]. The latter process leads to an exponential increase of the dark count rate with bias current, which further increases with temperature. This intrinsic behavior of superconducting nanowires has been observed, especially in the presence of defects or nanowire bends [113]. Other than shielding the system from background radiation [122] and reducing the electronic noise via appropriate filtering and low noise amplification, e.g. at cryogenic temperatures [123], it is highly beneficial to operate the detector at lower bias current. This helps to avoid a biasing regime where nanowire detectors are most sensitive to undesired superconducting fluctuations and thus result in minimal dark count rates. However, this preference for operating nanowire detectors at low bias current needs to be weighed against the desire for high detection efficiency, requiring high bias current. An optimal compromise in terms of noise equivalent power is typically achieved at the onset of the saturation regime (see Section 2.1), where low dark count rates and high detection efficiency are achieved simultaneously.

2.3 Recovery time and afterpulsing

After a detection event, the detector is temporarily not able to produce any electrical response. This time interval (dead time) is followed by a transient time needed for the detector to restore its full efficiency (reset time). The recovery time τ_r is the sum of these two time intervals and sets a limit to the effective maximum count rate a detector can support $R_{max} = 1/\tau_r$ [21, 124]. To assess an SNSPD's recovery time, it is instructive to consider the detectors decay time $\tau_d = L_K/R_L$ of the electrical output pulses, which is determined by the kinetic inductance of the device L_K and on the load resistance R_L of the electrical readout electronics (typically 50 Ω).

The kinetic inductance is directly proportional to the detector length and inversely proportional to the nanowire width [41]. Therefore, shorter detectors show lower kinetic inductance and therewith feature shorter pulse decay times resulting in faster detector recovery. While shorter detectors may be desirable for enabling high count rate devices, the shorter nanowire length will also lead to lower absorption efficiency and hence lower detection efficiency. However, embedding nanowires in optical resonant structures is one approach where bandwidth is traded off for simultaneously achieving fast detector response time and high detection efficiency in a nanophotonic device, as discussed in Section 4.2. Afterpulsing in SNSPDs is clustering of dark counts in the time domain and is mainly related to the presence of reflections in the electronic readout circuit [125, 126].

Afterpulsing and recovery time are typically characterized by acquiring the inter-arrival time distribution of detection events from which the second-order correlation function can be calculated [82, 127], as depicted in Figure 2B. This technique consists of illuminating the detector using a continuous wave (CW) laser and collecting the recorded counts with a fast oscilloscope or a field programmable gate array (FPGA) acquisition board to generate a histogram of the time delay between subsequent events. To properly model the detector response when operated near the maximum count rate, the contribution of more than one prior detection events shall be considered. To account for these nonlinearities, a higher order correlation model between time-tagged detection events has been proposed [128]. The purpose of this model, experimentally validated on semiconducting single-photon detectors, not only is restricted on the characterization of the timing response of the detector but also allows to obtain a more general detector calibration, which includes detection efficiency and dark count rate and can be applied for any binary detector, such as SNSPDs.

2.4 Timing uncertainty (jitter)

In addition to being able to operate a single-photon detector at high counting rate, it is also desirable to register events with low timing uncertainty, especially for timing correlation experiments. The relevant quantity, the timing jitter, describes the uncertainty in the time domain with which an electrical signal is registered after a photon was absorbed in the nanowire [22]. The timing jitter can be determined by using a pulsed laser source and collecting a histogram of the time delay between a trigger signal from the laser and the electronic readout signal of the detector [111, 129]. Trigger signals synchronous with the emitted laser pulses can, for example, be generated from high-speed photodiodes, which allow for taking full advantage of the high timing accuracy in the generation of ultrafast pulse trains with mode-locked lasers (typically <1 ps). The jitter performance

of an SNSPD fundamentally depends on three main contributions. The first one is an intrinsic contribution, which has been evidenced for bulk SNSPDs and has been associated to the superconducting fluctuations in the thermalization processes that take place from the initial photon absorption until an electrical output pulse is generated [22]. Evidence for such fluctuations was found with SNSPDs made from amorphous superconductors, where this contribution appears to play a significant role when the detector is operated at low bias currents (probabilistic regime), while it is less prominent when the detector is operated in the regime of saturated detection efficiency (deterministic regime) [130]. A second contribution, referred to as geometric jitter, is related to the variation in the position where a photon is absorbed, which results in an arrival time fluctuation of the nanowires voltage response at the counting electronics [22, 131]. Longer detectors experience higher geometric jitter, and it was observed that uniform illumination of a detector will reduce this contribution to the overall jitter value [131]. In waveguide integrated SNSPDs, the geometric jitter contribution is expected to be rather small due to the uniform illumination of the nanowire in the evanescent field of a nanophotonic waveguide, as well as the nanowire's short length as compared to meander-type SNSPDs. The third contribution to the overall detector jitter is associated with the SNR of the detector voltage pulse, which improves at high bias currents, where the corresponding output voltage is also higher, further depending on the readout electronics [129]. Typical jitter values <50 ps have been achieved with Nb-based detectors. Employing low-temperature amplifiers and readout electronics, low jitter values of 2.7-ps jitter at 400-nm wavelength and 4.6 ps in NIR wavelength have been recently demonstrated with 5-μm-long, 7-nm nominal thickness, NbN nanowires, with respective widths of 120 and 80 nm [94]. Interestingly, these performance values were shown to still be limited by the readout scheme. Hence, superconducting electronics could be designed to improve impedance matching between the detector and the RF readout circuit, thus allowing for further reducing overall device jitter. While current sub-10-ps jitter SNSPDs already offer exciting perspectives for practical applications, any further improvement of the detectors' timing accuracy will eventually allow for studying the intrinsic detector behavior and better understanding and exploiting the physics underlying the detection mechanism.

2.5 Spectral range

Superconducting nanowire single photon detectors provide high detection efficiency from UV to mid-infrared wavelengths [19, 112, 132]. As discussed in the Introduction, a cloud of quasiparticles is generated upon photon absorption in the nanowire, which in turn switches to a resistive state triggering a detection event. The quasiparticle concentration during the initial stages of the detection process depends on the ratio between the incident photon energy and the superconducting energy gap [35]. The higher the photon energy (i.e. shorter wavelengths), the more quasiparticles are generated, and it will be more likely to operate the detector in the deterministic regime. The detection efficiency will further depend on the relation between quasiparticle cloud size and nanowire geometry as current crowding and quasiparticle diffusion affect the performance [19]. Considering only the superconducting material specific properties, there is no lower limit for the shortest detectable wavelength. On the other hand, the longest detectable wavelength is determined by the superconducting gap and by the nanowire width. NbN and WSi nanowires have shown saturated spectral response up to 5.5 μm [112], evidently limited by the capability to fabricate (narrow) nanowires with higher uniformity. For waveguide-integrated SNSPDs, the spectral range of the detector is determined not only by material properties and geometry of the superconducting strip but also by the waveguiding material. Several material systems that are well suited for fabricating photonic integrated circuits have limited transparency windows. Silicon, for example, is a very popular choice for many integrated optics applications due to its high refractive index, which guarantees strong mode confinement inside a waveguide. However, silicon is only transparent for wavelength in the NIR spectral region and can therefore not take advantage of the full spectral bandwidth of waveguide-integrated SNSPDs. Alternative photonic integrated circuit material systems such as aluminum nitride (AlN) [133], silicon nitride (SiN) [111] and the more exotic polycrystalline diamond [115], however, feature extremely large optical transparency windows and have been demonstrated to be suitable for realizing high-performance SNSPDs, as discussed in Section 3.1. Among these materials, diamond is particularly attractive because it provides optical transparency from the UV to the mid-infrared. Beyond the material platform, an additional bandwidth limitation of waveguide-integrated SNSPDs arises from the waveguide geometry required for low-loss propagation of transverse electric and magnetic field modes (e.g. the waveguide cross-sections determine the maximum wavelength for which a propagating mode is still supported). Lastly, the mechanism for coupling light into an optical waveguide on a chip may underlie further bandwidth constraints, as it is, for example, the case when using optical grating couplers [134].

2.6 Photon number resolution

Superconducting nanowire single photon detectors are generally treated as binary threshold detectors for which PNR is not intrinsically possible, unless additional elements are introduced, for example, arrays of interconnected detectors [135–138] or by an opportune engineering of the electronic readout scheme [139]. However, at low bias current and under specific illumination conditions, a detector response can be observed only if several photons are absorbed simultaneously [30, 140–142]. In such a situation, the working point can be tuned to distinguish between the absorption of n photons or more, and less than n photons. When characterizing and using SNSPDs in this particular *modus operandi*, it is essential to choose suitable bias current and illumination conditions. This threshold detection regime is attractive to perform quantum detector tomography of the device under testing [143–146] or, for applications with faint lasers, adopting coherent tomography [16, 140].

2.7 Yield and scalability

A key advantage of integrated technologies is that they allow for realizing large numbers of devices on a single chip. Semiconductor industry development has demonstrated continued miniaturization of integrated electronic circuits while preserving their functionality, which has resulted in today's highly integrated electronic components. Photonic integrated circuits have been developed following similar technology and fabrication strategies. In this case, however, scalability (rather than scaling) is often referred to as the possibility to easily replicate photonic circuit elements in large numbers on the same chip. The minimal feature size of a photonic circuit is determined by the wavelength of the guided light, which constrains the minimal waveguide dimensions for which low-loss mode propagation in the material of choice (refractive index) is still guaranteed. Superconducting nanowire single photon detectors obey similar constraints but can be manufactured in reproducible fashion. Hundreds of waveguide-integrated devices are routinely fabricated on the same chip [147], and devices with up to 11 simultaneously working tungsten silicide (WSi) detectors have been reported [148]. In terms of device yield, amorphous materials such as WSi are more robust with respect to structural defects [82]. To the best of our knowledge, no systematic studies on degradation of detector performance parameters with time have been reported thus far. However, NbN nanowire detectors on SiN waveguides

Table 2: Key metric comparison for different waveguide-integrated detection technologies.

Key metric	"Detect Program" [84]	SNSPD (bulk)	SNSPD	TES	SPAD	TCSPC electronics
Timing jitter (FWHM)	<100 fs	<5 ps [94]	18 ps [102]	4.1 ns [150]	105 ps [151]	<10 ps [152]
Dark counts	<1/day	<10 cps [82]	<100 mcps [153]	Negligible [154]	~kcps [151]	–
Maximum rate	>10 Gcps	25 Mcps [82]	~Gcps [155]	~Mcps	~Mcps	25 Mcps [156]
Bandwidth	At least three of the following simultaneously: X-ray, UV, visible, IR, MWIR, LWIR	UV to MIR	UV to MIR	UV to MIR	UV to MIR (not simultaneously)	–
OCDE (at NIR)	>99.9%	93% [82] (SDE)	91% [102]	43.7% [154][a]	5.27% [151]	–
PNR	$>1–10^3$	Only using spatial/time multiplexing	Only using spatial/time multiplexing	5 photons [154]	Only using spatial/time multiplexing	–
Operating temperature	Room temperature	<4 K	<4 K	<100 mK	80 K	–

[a]In the cited work, a cascade of three detectors has been used to achieve a total detection efficiency of 79.2%. Here, the maximum achieved efficiency per single TES detector was reported. As in Table 1, in the first column, we report the reference metric proposed within the DARPA "Detect" program. For comparison, in the second column, we show the state-of-the-art performances for bulk SNSPD where, in this case only, the reported efficiency is the system detection efficiency (SDE). In addition, the jitter is reported for low-noise low-temperature amplifiers, while for integrated SNSPDs, the jitter has been measured using room-temperature amplifiers. In the last column, we report also some information on commercially available time-correlated single-photon counting electronics.

capped with a passivation layer of hydrogen silsesquioxane (HSQ) showed no change in critical current and detection efficiency over the course of 3 years. For NbN nanowire detectors on silicon-on-insulator (SOI) waveguides, a 97% fabrication yield was inferred from room-temperature measurements of more than 600 SNSPDs across two chips [149]. As these studies were performed in a research environment, it may be expected that fabrication yield of hybrid superconducting-photonic circuits will not be a limiting factor when resorting to state-of-the-art semiconductor industry fabrication routines.

2.8 Comparison with other waveguide-integrated detectors

To summarize the previous sections and put waveguide-integrated SNSPDs in perspective, we presented a comparison of crucial detector performance parameters in Table 2. We compared fundamental DARPA key metrics with the state-of-the-art for on-chip detector technology. As the detector output consists of electric signals, we also included information on state-of-the-art commercial time-correlated single-photon counting electronics because it may ultimately limit some of the performance characteristics of an overall photon counting system.

3 Material choices for waveguide integrated detector systems

The optical properties of the integrated platform and the material properties of the superconducting film used for the realization of superconducting-nanophotonic hybrid detector have significant influence on the final performance of such devices. In Table 3, an overview of the application of SNSPDs for different photonic platforms was reported. The following sections are dedicated to a review and a comparison among the commonly used photonic platforms and superconducting materials for waveguide integrated SNSPDs.

3.1 Integrated photonic platforms

In analogy with electronics, integrated optics has been acknowledged to be one of the most promising enablers for successfully implementing optical quantum technologies [4, 5]. A vast range of material platforms has been explored for integrated photonics [174]. To date, for a variety of them, the successful integration of superconducting nanowire single-photon detectors has been shown. In Figure 3A, we showed an atomic force microscope (AFM) scan of the nanowire detector pattern atop of different material substrates. The superconducting film is typically a few nanometers thick and the AFM measurement has been performed on the exposed e-beam resist. The difference between the materials is mainly given by the refractive index, which determines mode confinement and the transparency window that, in turn, defines the optical bandwidth. In fact, as also depicted in Figure 3B, each material shows a specific transparency window, in which light can be guided without being absorbed. Absorption in the cladding material influences also the optical bandwidth; therefore, the transparency window of SiO_2 and MgO are reported as well.

3.1.1 Silicon-on-insulator

Silicon has a long tradition in integrated electronics and represents today one of the most used technological platform for integrated photonics. Through the advent of SOI, high-density devices with foundry-ready CMOS technology can be realized nowadays. Silicon has a very high refractive index (n = 3.45 at 1550 nm) allowing tight light confinement and very low bending losses, which results in the

Table 3: Overview of the realized waveguide-integrated SNSPDs for different photonic platforms.

	NbN	NbTiN	WSi	MoSi
Si	[102, 147, 155, 157, 158]	[106]	[148]	[159]
SiN	[105, 111, 142, 160, 161]	[75, 149, 153, 162, 163]	[164, 165]	–
GaAs	[101, 136, 137, 166–168]	–	–	
AlN	[158]	–	–	–
LiNbO3	[169]	–	[170]	–
Diamond (polycrystalline)	[115, 171, 172]	–	–	–
Diamond (single crystal)	–	[173]	–	–

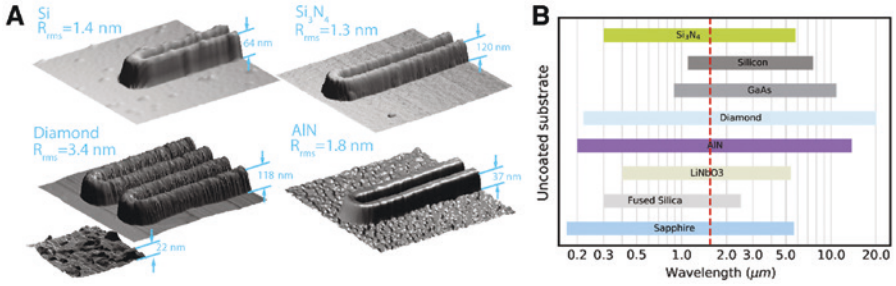

Figure 3: Material platforms for waveguide integrated SNSPDs.
(A) AFM scan of NbN waveguide-integrated SNSPDs on different platforms. The scan has been made on an area of 1×1 μm on the E-beam resist (hydrogen silsesquioxane) used for the nanowire pattern exposure, before etching the nanowires. For each micrograph, the rms surface roughness of the waveguiding material is reported. The final resist height depends on the chemical concentration, the spincoating parameters and the dose used for the exposure. (B) Transparency window for different substrates adopted in integrated optic technology.

possibility of integrating dense optical structures [2]. One of the main limitations in the application of silicon photonics is that, due to its small band gap (1.1 eV), it is not possible to guide visible light in silicon. This represents a major drawback especially considering that for most applications in biology and the life Sciences, investigation in the visible spectra is essential. Efficient single-photon generation and detection on a photonic chip are two main challenges for the integrated photonics community. Being able to efficiently generate and detect single-photon is a key aim for the photonic community but would be of limited use without an established photon manipulation technology. In this context, a further limitation of Si is related to thermal instability processes due to two-photon absorption (TPA) and free carrier absorption, which limits fabrication devices with active functionalities [175–177]. In addition, because of its centrosymmetric structure, Si does not provide the electro-optic effect, which would enable ultrafast on-chip modulation of light and phase shifts.

3.1.2 Silicon nitride

Between different larger band-gap materials, silicon nitride is an attractive alternative to silicon. Among the different substrates, SiN matches well to the crystal phase of NbN and best film quality has been obtained so far [178]. However, silicon nitride often suffers from intrinsically high film stress, which can degrade the film quality and cracking limits the patterning area for photonic structures. Using adapted low-pressure chemical vapor deposition (LPCVD), it has been possible to realize low-stress films overcoming this limitation [179]. Nowadays, SiN is a well-established material for electronics application and similarly to SOI can be easily purchased commercially. The refractive index of SiN is smaller compared to SOI (~2 at near-IR wavelengths), limiting the confinement of the propagating light field. Nevertheless, improved fabrication techniques allow to obtain extremely low surface roughness and ultra-low-loss waveguides can be achieved [180]. Different passive devices can be realized including Mach-Zehnder interferometers, high-quality factor ring resonators and filters, Bragg filters and photonic crystal cavities [181]. Due to its good thermal conductivity, the successful application of thermo-optical modulator and phase shifter on SiN has been demonstrated [182, 183]. Despite showing promising performance, these devices are typically slow and are not perfectly suitable for low-temperature applications, which is essential to sustain the superconductivity of the detectors [184].

3.1.3 Gallium arsenide

Among III–V semiconductors, thanks to its strong second order nonlinearity, GaAs is an established material for integrated photonics [7]. Low-loss waveguides can be realized in GaAs. GaAs has also been the first material adopted for successfully integrating on-chip superconducting single-photon detectors [101]. GaAs further provides extremely good mechanical properties. One of the major advantages of this material is that it allows integration of quantum dots, which is nowadays a reliable and scalable source of single-photon [185–187]. Opto-mechanical and electro-optic effects can also be exploited for on-chip phase modulation [188, 189], making this material extremely appealing as a monolithic platform for quantum optical applications. Despite the excellent mechanical properties, the small band gap of GaAs does not allow to access the visible light range. Furthermore, GaAs suffers from thermal fluctuation effects due to TPA at infrared wavelengths, as also observed with silicon.

3.1.4 Aluminum nitride

An interesting material that has been successfully adopted as an alternative platform is AlN. AlN is a semiconductor with one of the largest band gaps of 6.2 eV, high electro-mechanical coupling strength and large piezoelectric coefficients. This material is commonly used in micro-electro-mechanical systems (MEMS) technology but is also emerging as an attractive platform for integrated optics [190]. Acousto-optic devices based on the piezo-electric effect can be fabricated in a scalable monolithic fashion [191], and thanks to its non-centrosymmetric structure, an electro-optic effect has been exploited for the fabrication of modulators and phase shifters. These devices, thanks to their low dissipation, can be adopted also for low-temperature applications [192, 193]. In addition, second harmonic generation and parametric down conversion have been demonstrated, making this material a promising alternative for on-chip generation of photons [162, 194].

3.1.5 Lithium niobate

Because of its strong optical nonlinearity, lithium niobate (LiNbO3) has been widely used in integrated quantum optics [195, 196]. Waveguides can be realized by proton exchange or Ti diffusion techniques [174, 195] with very low propagation loss. LiNbO3 represents a complete platform for single-photon pair generation, and thanks to its large electro-optical coefficient, low-dissipation high-speed routing devices can be fabricated [197]. LiNbO3 is a large band-gap material (4 eV) and allows broadband applications from UV to far IR. Integration of superconducting detectors on LiNbO3 waveguides is still in progress, but its successful realization would represent an important enabler for further progress in integrated quantum technology [169, 170].

3.1.6 Diamond

Diamond deserves also an honorable mention when considering the good candidate platforms for integrated photonics. Similarly to AlN, diamond has an extremely wide band gap, 5.45 eV, and its transparency window spans from the UV into the far infrared. Diamond is known to be the most mechanically strong bulk material with a young modulus roughly six times higher than Si. Diamond has been shown to be a versatile material for opto-mechanical applications [198–200]. Phase shifters and modulators have been successfully demonstrated [201]. A big challenge in diamond nanofabrication lies in realizing devices in a scalable fashion using single crystal diamond, especially because of the difficulties to fabricate large area structures. To overcome this requirement, polycrystalline diamond directly deposited on wafer-scale substrates has been successfully adopted, allowing to realize large area nanophotonic circuits [200]. Diamond is also a chemically inert and biocompatible material. In addition, the possibility to access also the shorter wavelength regime makes this material very suitable for biological and natural Science investigations [202]. For quantum application, diamond can host color centers and represents a ready platform also for single-photon generation [203]. A limitation on adopting wide band-gap materials is the transparency of the substrate, which is often SiO_2. Alternative substrate stacks have been introduced, for example, diamond on AlN, which allows to access also deep UV and infrared wavelengths [204].

To summarize, different optical substrates that can be adopted for single-photon generation and routing of light and detection have been presented. To exploit the best performances of each material, interconnection technologies, such as photonic wire bonding, could allow to realize hybrid architectures by combining different platforms [205].

3.2 Superconducting materials for integrated SNSPDs

NbN, traditionally employed in radiation detection bolometers [206], was the first superconducting material used for single-photon detection in both free-space [30] and waveguide-integrated approaches [101, 102]. To enhance some of the functionalities of SNSPDs, during the last few years, many other materials have been investigated. In this section, we will review the most promising materials adopted for on-chip application.

3.2.1 Nitride-based superconducting detectors

An attractive advantage of NbN is the possibility to deposit very thin films (4–5 nm) while maintaining a high superconducting critical temperature. The critical temperature of bulk NbN lies between 14.7 and 16 K [207, 208], while for ultra-thin films (2–5 nm), it is in the range between 7 and 11.5 K [209], allowing the operation of the detector in its superconducting state already at helium bath temperatures, which can be easily reached with less expensive

Table 4: Comparison between the main superconducting materials used for single-photon detectors.

Material	NbN	NbTiN	WSi	MoSi	MgB2
Bulk $2\Delta_0$ (meV) $\{2\Delta_0/k_bT_c\}$	4.92 {3.53} [210]	4.52 {3.72} [211]	1.52 {3.53} [107]	2.28 {3.44} [107]	3.6 (π)-13.6 (σ) @4K {1.06 (π)-4 (σ) } [212]
Bulk Tc (K)	14.7–16 [208]	14.1 [211]	5 [107]	7.69 [213]	39 [214]
Tc (K)	11 (5 nm) [209]	13 (~4 nm) [215]	3.4 (~4.5 nm) [82]	~6.5 (10 nm) [159]	21.95 K (15 nm) [216]
Jc (MA/cm^2)	6–7 @ 4.2 K [217]	3 @ 1.6 K [153]	0.74 @ 120 mK [82]	3.3 @ 0.8 K [130]	2.7 @ 4 K, 1.1 @ 11 K [216]
ρ (μΩ · cm)	400–600 (5–7 nm, 20 K) [83]	93 (4 nm, 20 K) [218]	200 (4.5 nm, 300 K) [82]	~200 (4 nm, 10 K) [219]	~40 (15 nm, 30 K) [216]
Relaxation time (ps)	20–50 [16]	n.a.	80–800 [24]	n.a.	n.a.
IQE sat. at 0.8Ic (NIR)	Yes[a] [83]	No	Yes [82]	Yes [130]	No

[a]Only with films with engineered disorder.

cryocoolers. As shown in Table 4, NbN shows a high normal state resistivity [220] and critical current density [217], resulting in a better SNR of the electric response pulse and a reduced electronic noise jitter. In comparison to other materials, NbN exhibits a short quasiparticles relaxation time (20 ps) [16, 23, 221]. Such fast thermalization process is desirable, as it allows for a short recovery time of the detector. In integrated optics technology, reproducibility on a large scale is a fundamental requirement. NbN, as polycrystalline film, is affected by structural inhomogeneities and substrate mismatch, limiting both the range of waveguiding materials on which it can be deposited and the overall deposition yield for large areas [222]. Although with well-matched substrates, room-temperature deposition can be adopted [223], in most cases, to improve the crystal phase of the deposited film, technologically demanding high-temperature deposition (up to 1200 K) is required [169, 224].

For improved deposition homogeneity, niobium-titanium-nitride (NbTiN) has been adopted also for on-chip detectors [163, 225, 226]. The addition of Ti results in a reduced normal resistivity, thereby a lower kinetic inductance, and therefore in a higher achievable maximum count rate [227]. Better homogeneity also leads to a reduced dark count rate with respect to NbN detectors [225]. A detailed comparison between these two nitride-based materials [228] hints towards better yield for NbTiN detector films. In addition, lower kinetic inductance and higher switching current result in better electronic noise jitter performance with NbTiN. While operating temperature and timing characteristics (lower jitter and recovery time) represent the major advantage of nitride-based detectors, because of the high sensitivity on the deposition parameters and on the structural homogeneity, it remains, nevertheless, very challenging to achieve saturation of the internal quantum efficiency. Amorphous materials, silicides, in particular, have been investigated to overcome this limitation. As discussed in detail in the next section, higher fabrication yield and saturated detection efficiency also at low bias currents have been demonstrated. Interestingly, recent results [83] evidenced saturation of the internal quantum efficiency in NbN detectors with increased structural disorder.

3.2.2 Amorphous silicides

A very large set of silicides for single-photon detection has been intensely studied in recent years. Among these, tungsten silicide (WSi), molybdenum silicide (MoSi) and niobium silicide (NbSi) showed better performance. One of the main advantages of these materials is the possibility of depositing them at room temperature, enabling bottom/up fabrication where the nanowire is deposited and patterned on top of an existing photonic circuit. Furthermore, as no crystalline structure matching is needed, they can be deposited on a wider range of substrates and waveguiding materials on respect to polycrystalline films. Silicides exhibit also a relatively small superconducting band gap on respect to nitrides, allowing to generate a higher quasiparticles density for the same absorbed photon energy. In addition to this, the experimentally characterized quasiparticles relaxation time in WSi is longer than for NbN, as shown in Table 4. These two factors could be indicative of a different detection dynamic between amorphous silicides and polycrystalline nitride films and might explain why, in silicides, the quantum efficiency reaches a saturation regime already at low bias currents. The major drawback of these materials is the lower critical temperature, which typically requires operating the detectors below 2 K. As also reported in Table 4, critical current density and room-temperature resistivity are typically smaller in comparison with nitride-based materials, with repercussions on the electronic SNR,

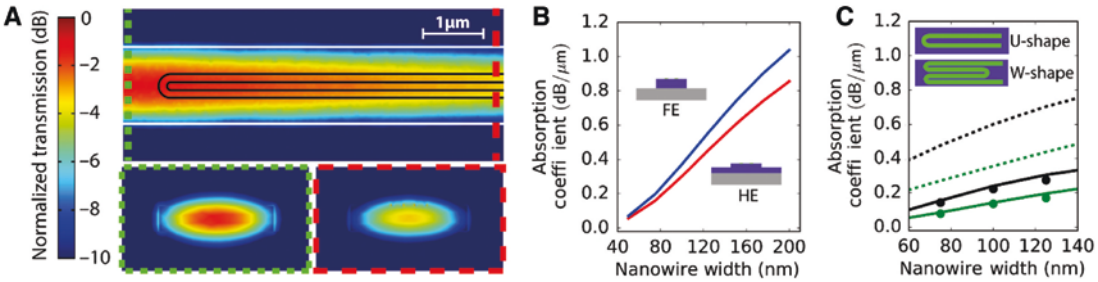

Figure 4: Absorption engineering.
(A) Simulation of the transmission of TE-like mode propagating into an SOI waveguide in the presence of a U-shape nanowire detector. The green inset shows the mode profile in the absence of the detector and the red inset shows the mode profile in the presence of an NbN nanowire. The FEM simulation has been performed using COMSOL Multiphysics considering a 100-nm-wide U-shape nanowire atop a fully etched Si 220-nm waveguide. (B) Simulated absorption per unit length at different nanowire width for a 340-nm-thick SiN on SiO_2 waveguide. Because of the better mode profile overlap with the nanowires, fully etched (FE, blue curve) waveguide exhibited a better absorption characteristic than half-etched (HE, red curve) waveguides did. (C) Comparison of the absorption coefficient for single meander (U-shape, green) detectors and double meander (W-shape, black) detectors on diamond on SiO_2 platform. In this configuration, because of their better coupling with the nanowire, TM-like modes (dashed lines) are better absorbed than TE-like modes (solid lines). For TE-like modes, experimental results using a balance splitter technique [103] are also reported (circles), following [171].

causing a higher timing jitter. Recent results using MoSi [130] showed critical currents of 37.5 μA at 0.8 K and a saturated internal quantum efficiency at 90% of the switching current. By adopting cryogenic amplifiers, best jitter values of 26.1 ps have been reached close to the switching current. The use of amorphous materials in combination with integrated photonic platforms is still in progress. A promising result is the implementation of large detectors array on SiN/Si platform for the characterization of fully integrated laser sources [148]. Also MoSi detectors on SOI waveguides have been fabricated, although these devices have been characterized only through perpendicular illumination [159]. In addition, the optimization of WSi on LiNbO3 waveguide detectors has recently been proposed [170].

3.2.3 High-temperature superconducting materials

The need for operating superconducting detectors at low temperatures represents an unquestionable limiting factor. Substantial efforts have been undertaken to fabricate ultra-compact cryogenic systems, which can be hosted in a laboratory rack [229, 230]. Nevertheless, the possibility of adopting higher temperature detectors would be of great advantage for the application of such devices. High Tc materials, such as YBCO, have also extremely small relaxation times (1 ps), which could potentially allow to implement extremely fast detectors. However, to date, it has been possible to demonstrate photocounting at 1550 nm only with MgB2 at an operating temperature below 11 K using standalone detectors [216].

4 Nanophotonics for detector performances engineering

In this section, we reviewed the most interesting applications for the enhancement of the detectors performances. The first two paragraphs are dedicated to the methods and technologies for the enhancement of the absorption efficiency. The third paragraph is dedicated to a method to pre-select the best performing devices and transfer them on desired photonic platform. The last two sections are dedicated to the realization of architectures for PNR and spectral sensitivity.

4.1 Efficiency absorption engineering

A photonic waveguide consists of a ridge structure made of a dielectric material with refractive index higher than the surroundings refractive index [231]. Light is two-dimensionally confined in this structure and free to propagate along a third direction. The intensity of the travelling electric field does not abruptly vanish at the waveguide boundaries but decreases exponentially with distance. This evanescent coupling depends on the refractive index contrast between the waveguiding material and the surrounding environment. It is therefore possible to let the evanescent field interacting with external objects for sensing applications [202, 232] and by controlling the evanescent coupling between nanowires and waveguides the absorption probability can be optimized. As mentioned in the Introduction, in fiber-coupled detectors, light falls under normal incidence onto the nanowire detector and

the absorption occurs only in the few-nanometer-thick superconducting material. Although optical stacks have been used to overcome this limitation [79], in general, for sufficient absorption efficiency, long meanders must be used [82], thus increasing the detector recovery time [21]. On integrated photon platforms instead, the evanescent coupling occurs longitudinally with respect to the electric field propagation direction, as depicted in Figure 4A. This is one of the major advantages of the waveguide-integrated architecture, as the absorption probability density can be higher than in the fiber-coupled configuration and shorter nanowires can be used, guaranteeing the combination of high detection efficiency, fast response and small footprint. In Figure 4B, C, we report a comparison of the absorption coefficient per unit length for different waveguide and detector geometries. Simulation results of Figure 4B show that fully etched structures exhibit a higher absorption compared with half-etched structures. This can be explained considering that, in the latter case, the propagating field is more confined towards the substrate and therefore the overlap integral between propagating mode and nanowires placed atop the waveguide is smaller. Besides increasing the detector length, the absorption efficiency can be optimized also by adjusting the nanowire width. On the other hand, an excessive increase of the wire width might limit the internal quantum efficiency of the device [111] or lead to a strong reduction of the device kinetic inductance, thus increasing the probability of observing latching [42]. In Figure 4C, the polarization dependence of the absorption efficiency is also shown. When the nanowire is placed atop the waveguide, transverse magnetic TM-like modes couple more strongly to the nanowire. Better absorption for transverse electric TE-like modes can be achieved by using longer detectors in a compact W-shape double meander geometry or, alternatively, by placing the nanowire at the side of the waveguide. In analogy to fiber-coupled detectors [79, 233], enhancement of the absorption efficiency has been obtained by embedding the detector in a photonic cavity or a resonant circuit [104, 106, 155]. As discussed in the next section, the cost of this improvement is a limited optical detection bandwidth.

4.2 Coherent perfect absorption (CPA) for near-unit absorption efficiency

In a travelling-wave configuration, the absorption efficiency depends on the coupling length between the detector and the travelling mode. Therefore, increased absorption efficiency requires long or wide detectors. While the latter case has negative impact on the internal quantum efficiency [111], long detectors result in larger footprint, longer recovery time and increased probability of imperfections, which could limit the detectors operation. In 2014, Akhlaghi et al. [106] proposed a CPA scheme to overcome the trade-off limitation between absorption efficiency and reset time of SNSPDs. As initially introduced by Chong et al. [234], CPA is an interference-assisted absorption effect, which, in a lossy system, allows complete dissipation of the input optical power of two counter-propagating beams illuminating a dissipative medium. In the

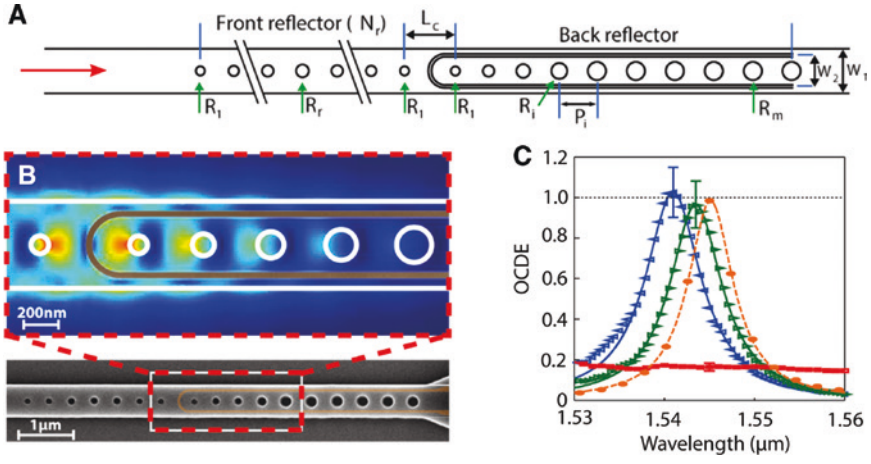

Figure 5: Perfect absorber approach for SNSPDs.
(A) Model of the photonic crystal cavity for achieving near-perfect absorption as proposed in Ref. [106]. (B) SEM picture of the fabricated architecture. In the inset is presented the simulated profile of the electric field on the waveguide surface. (C) Measured OCDE at $0.9I_{sw}$ for two different devices (blue and green triangles). Orange circles represent the simulated absorption efficiency, and the red squares are the measured OCDE in the absence of the micro cavity. Figure adapted with permission from [106] © Springer Nature.

configuration proposed by Akhlaghi et al. [106], destructive interference occurs between the directly reflected light at the front reflector and multiple reflections generated by a cavity. The cavity, depicted in Figure 5A, B, consists of two integrated photonic crystal elements acting as mirrors, realized by etching a series of holes into the Si waveguide. The back mirror is designed to be perfectly reflective; therefore, no light is transmitted through the cavity but can be either reflected or absorbed in the nanowire. The front mirror is designed such that, under resonant conditions, all incident light is dissipated inside the cavity. For negligible scattering losses, the nanowire represents the only dissipative medium and near-unit absorption efficiency at the detector can be achieved. In a real scenario, scattering losses are present inside the cavity and negatively impact the achievable absorption efficiency. The main sources of scattering losses are impedance mismatch between the Bloch and the guided modes at the interface between photonic crystal cavity and waveguide, and the propagation losses to the substrate. Optimized tapering of the input mirror and free-standing structures can therefore be respectively adopted to minimize these contributions. The simulated absorption in resonance is 98.4%, as depicted in Figure 5C (orange circles). The main limitation from obtaining unitary detection efficiency is due to losses to the substrate, which has been calculated as 1% lost contribution. The measurement data for the realized device are shown in Figure 5C. It is possible to observe that the best OCDE measures are $102 \pm 8\%$ at $0.9I_{SW}$ resonance and at the temperature of 2.05 K (blue triangles). In the absence of CPA, the detector efficiency has been measured to be below 20% (red squares). As expected, the detectors' functionality is limited in bandwidth, because of the presence of the cavity, but the filtering effect of the cavity helps to minimize the absorption of stray light, resulting in a reduced dark count rate. In addition, defect-induced dark counts are reduced by adopting compact size detectors. In this configuration, the dark count rate, with sealed optical windows, has been determined to be 0.1 cps. This almost-ideal detection efficiency performance is accompanied also by a strongly reduced reset time. For comparison, similar efficiencies in a standard configuration could be obtained only with a 160-μm-long U-shape detector with, consequently, 4.5 times slower recovery time. Fast detectors, with >Gcps count rate, would enable very sensitive time-resolved live imaging applications and high rate communication or cryptography. The CPA approach allows a break in the recovery time and absorption efficiency trade-off dilemma, allowing to design and fabricate very compact devices. Following a similar approach, by embedding a 1-μm-long NbN microbridge in a one-dimensional SOI photonic cavity, it has been possible to obtain recovery times below 500 ps, which could potentially enable detection rates on the order of the Gcps. Due to high scattering losses, the absorption enhancement was limited to an upper total OCDE of 30% [155]. A further improvement of the structure by adopting a 2D photonic cavity allowing a reduction of out-of-plane losses allows to reach almost 70% OCDE by maintaining high timing performances [157].

4.3 Flip-chip SNSPDs transfer technique for complex functionalities with high yield

Because of the need for complex architectures, which do not always require accessible high-end fabrication facilities, a recent trend in research is to refer to foundries for the fabrication of integrated photonic circuitry. It is therefore indispensable to develop deposition methods compatible with a back-end-of-the-line step. This is especially true for NbN, which for high-quality films, i.e. high internal quantum efficiency, requires high-temperature deposition. Najafi et al. [158] introduced a micrometer-scale flip-chip transferring process that enables the integration of SNSPDs into existing circuitry with high yield. NbN SNSPDs are, in a first step, realized on a thin (200–300 nm) SiN film on Si. After a pre-selection step in which the detectors are characterized to identify and select the best performing devices only, the Si substrate is etched, leaving only a thin flexible membrane with SNSPDs and electrical contact pads for their electrical connection. Subsequently, using a tungsten probe and PDMS as an adhesive, the selected detectors are transferred to the target waveguide. The contact pads of the detectors are connected to complementary gold pads on the hosting circuit with a final alignment precision, using an optical microscope, better than 1 μm. A sketch showing the transfer technique is reported in Figure 6A. To show the potentiality of this technique, an on-chip time-energy correlation measurement of entangled-photon pairs has been performed. For this experiment, 1560-nm photon pairs have been generated by an off-chip PP-KTP spontaneous parametric down conversion source, separated at a polarization beam splitter, collimated into two different fibers and coupled onto the photonic chip on a low-temperature stage (2.8–3 K). The photonic circuitry consists of two two-port directional couplers on which a total of four detectors have been integrated using the flip-chip process transferring technique, as depicted in Figure 6B. The pre-selected detectors exhibit an average OCDE of $52 \pm 6\%$ and a FWHM jitter (using room temperature amplifiers) between 39 and 57 ps at 1550 nm. Time-resolved correlation measurements

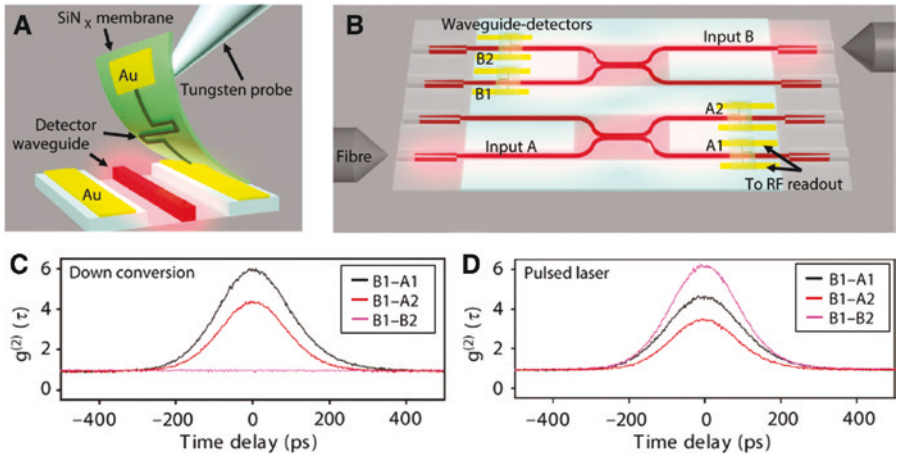

Figure 6: Transfer protocol for hybrid detector devices.
(A) Sketch of the pick and place technique for transferring a detector onto a hosting chip with photonic waveguide and contact pads. (B) On-chip interferometer with four waveguide integrated detectors and two directional couplers. (C) Coincidence counts at different delay times for different channel combinations for the off-chip entangled-photon pair source and (D) for a mode-locked pulsed laser with similar output power that of the pairs source. Figure adapted with permission from [158].

have been performed between the two input channels A and B. A final system timing uncertainty of 200 ps has been achieved, and as expected for a photon pair source, antibunching has been observed from A and B channels but not within the individual ones, as shown in Figure 6C. Using a classical light pulsed mode-locked laser source, instead, correlation between all the channels was observed (see Figure 6D). All the transferred devices showed the same performance as in the pre-selection stage, allowing to obtain a working photonic architecture, including detectors, with, in this case, 100% yield. The SiN membrane is flexible and can be potentially adopted to other surfaces. Successful integration on Al on sapphire waveguides has been demonstrated using this technique, which could also serve as a promising approach for transferring detectors on LiNbO3 substrates. The proposed method has been demonstrated to be an effective technique to pre-select working detectors and transfer them onto pre-existing photonic circuitry.

4.4 SNSPDs array for photon number resolving detection

PNR capability, i.e. the possibility of retrieving the information about the number of photons that have been absorbed after the detection of an event, would be of great advantage for many applications; photon number statistics [235], quantum communication [236] and cryptography [237] are only few examples. For true-photon number sensitivity, transition edge sensors (TES) are typically employed [238]. The response of a TES is directly dependent on the amount of absorbed energy and therefore to the number of incident photons. The main drawback of TES is that they are based on the thermal response and their recovery time is in the order of microseconds. Differing from TES, superconducting single-photon detectors are threshold detectors, meaning that they are only capable to distinguish the presence of a photon or not [30, 140, 142]. Therefore, even if the final response is binary, SNSPDs can discriminate in a threshold mode the presence of many photons. On the other hand, this multiphoton sensitivity is typically inefficient and not truly number-resolving. True PNR can therefore not be achieved intrinsically by SNSPDs. Yet, integration with photonic architectures can help to overcome this limitation by approaching almost-true PNR. As proposed by Sahin et al. [137], by creating a multiplexed array of integrated superconducting nanowire single-photon detectors atop the same waveguide, it is possible to probabilistically discriminate the number n of photons present in an incoming pulse. For an increased number N of detectors in the array, if $N > n$, there is a high probability that the absorption occurs in a sparse way, such that, with each detector, only one photon is absorbed [239]. This technique is not absolute, as it requires *a priori* estimation of the maximum number of photons present for each pulse to establish which would be a proper number of detectors in the array. Parallel and serial configurations [136, 239] can be adopted to achieve an output signal very similar to the more traditional TES response, with the main advantage of being two orders of magnitude faster than TES, because of the short SNSPDs' recovery time. In Figure 7, a schematic of the integrated series array proposed

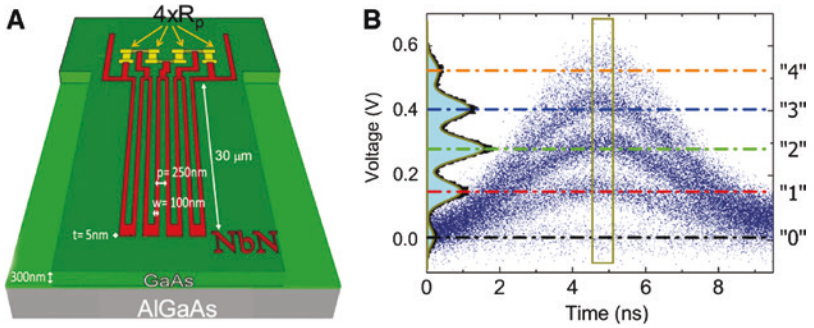

Figure 7: Photon number resolving SNSPDs.
(A) Waveguide-integrated photon number resolving detector with series configuration. (B) Persistence map of the detector output. Up to four-photon discrimination has been achieved. It can be observed that SNSPDs allow to improve the recovery time of few orders of magnitude with respect to TES. Figure adapted with permission from [137] ©AIP Publishing.

by Sahin et al. [137] is depicted with an example of the output signal. For this proof-of-principle experiment, a PNR up to four photons has been achieved. Alternatively, time-multiplexing using long ring resonators and ultrafast detectors can be employed for PNR [240]. In this case, the working principle is not based on the spatial distribution of the photons. Instead, the incident pulse is divided into N weak pulses separated by a time interval Δt, thus limiting the overall timing performances. For $N > n$ and Δt bigger than the detector recovery time, it is possible to discriminate the number of incident photons. On-chip delay lines can be readily achieved using integrated ring or spiral structures [241].

4.5 On-chip single-photon detection with spectral sensitivity

The attractive characteristics of SNSPDs can be of great interest in the life Sciences. Spectroscopy techniques, such as FRET [242] and FLIM [243], allow the lifetime monitoring of how molecules interact and communicate with each other, enabling the investigation of the functionality of the cells and their fundamental components. Solid-state detectors or photomultiplier tubes [244] are typically used for detecting weak emission of light in these experiments. For superior timing resolution and high speed, superconducting nanowire single-photon detectors would represent an attractive alternative suitable solution. Well-performing detectors are indeed a necessity but not a sufficient requirement. Life Science applications require also to resolve spectral information of the system under investigation. In this section, we review two different approaches that exploit the best performances of detectors, in terms of detection efficiency, speed, timing response to achieve energy resolution in very compact and well reproducible devices. The first approach consists of the integration of wavelength discriminating photonic circuitry with detectors [105], while the second approach combines the unknown weak signal with a local oscillator to achieve near quantum limited spectral sensitivity [245]. Thanks to its large transparency window, from the visible to the NIR, and low losses, silicon nitride is an attractive platform for spectroscopic applications; therefore, both experiments presented here have been realized using SiN on SiO_2. An on-chip single-photon spectrometer has been realized [105] by combining an arrayed waveguide grating (AWG) structure [246] with eight superconducting detectors at the output. A representation of the structure is shown in Figure 8A. AWGs are, nowadays, used for wavelength division multiplexing (WDM) in photonic networks and consist of two star couplers [247] connected by multiple waveguides of different length. Star couplers are devices capable of redistributing the optical power with low loss from one or more input waveguides to one or more output waveguides. The first coupler serves therefore as a low loss multiport splitter. The signal is injected to an array of waveguides with precisely designed length to guarantee a constant phase shift increment from one waveguide to the other. At the combining star coupler, the waveguides array is condensed to few output waveguides. Thanks to the phase shift occurring within the array grating, the travelling waves will interfere at the output coupler, leading to a spatial redistribution of the input spectrum so that, for each output channel, only a portion of the original bandwidth will be transmitted. By placing a detector at each output port, it is then possible to achieve spectral information of extremely weak light signals. One single-photon spectrometer at the NIR range (1550 nm) with 24-nm spectral bandwidth and resolution of 2.2 nm and one spectrometer in the visible range (738 nm) with 60-nm

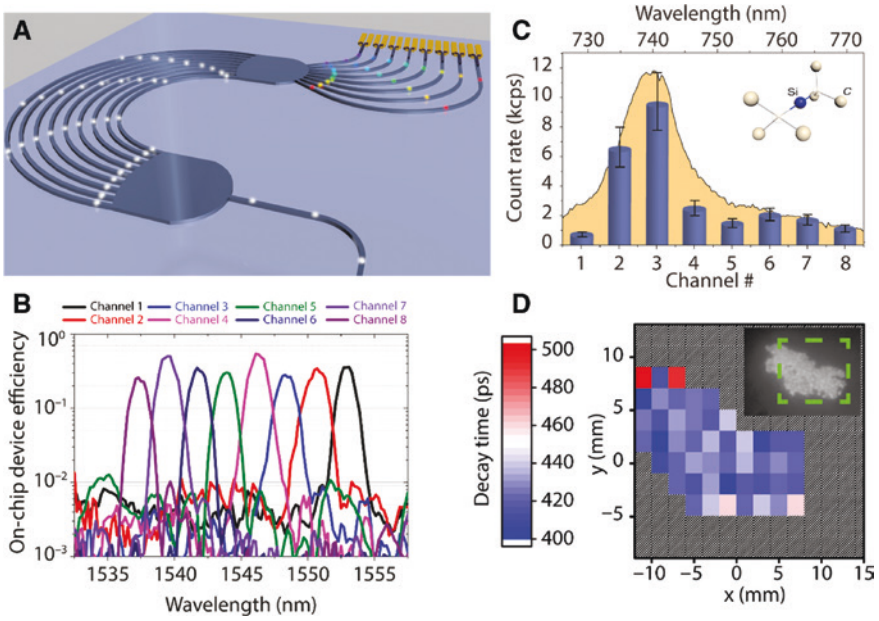

Figure 8: Integrated single photon spectrometer.
(A) Sketch of the on-chip single-photon spectrometer using an AWG connected to eight SNSPDs detectors. (B) On-chip device efficiency as a function of the wavelength. The detectors were biased at $0.9I_{sw}$. (C) Emission spectrum of SiV color centers in diamond as recorded by the eight-channel visible-range on-chip spectrometer (blue bars). Yellow represented the emission spectrum obtained with a conventional spectrometer. (D) Map of the fluorescence lifetime of the SiV centers cluster. In the inset is shown an optical micrograph of the cluster under test. In green is indicated the area scanned for the lifetime map. Figure adapted with permission from [105] © OSA Publishing.

spectral bandwidth and a final resolution of 6.4 nm have been realized. In this experiment, the number of available channels in the measurement system was limited to eight; therefore, the spectrometer has been designed with eight output ports only. In principle, the number of output channel can be increased to achieve a higher resolution or bandwidth. For short wavelength applications, especially, the main limitation of the number of output channels is the fabrication resolution. In fact, to avoid signal leakage, output ports should not overlap. In Figure 8B, we show the response of the eight-channel SPS in the near-IR range. A comparison with the room-temperature characterization of the device, performed using output grating couplers, indicates a blue-shift of 1 nm. This shift is due to a thermal change of the refractive effective index of the structure after cool down. The on-chip efficiency of the device, which takes into account the AWG losses and the detectors OCDE, was determined to be at 18% for the NIR device and 20% for the visible spectrometer. Concerning the detector characterization, an average detection efficiency of 60% and a 3-ns recovery time were achieved. The system timing jitter, with room-temperature amplifiers, was determined to be of 50 ps close to the switching current for both wavelengths regimes. The functionality of this device has been successfully tested by characterizing silicon vacancy (SiV) color centers in diamond, which are promising candidates for labeling in biological tissue and for single-photon emission [248]. The zero photon line (ZPL) for this sample is at 738 nm, i.e. at the central wavelength of the visible range SPS. In Figure 8C, the fluorescence spectrum of several SiV centers embedded in a nanodiamond cluster was shown. The broad spectrum is related to the wide emission window at room temperature and is consistent with the spectrum recorded with a conventional spectrometer. The scanning capabilities for the confocal microscope allowed to realize a map of the nanocluster emission spectrum. The combination of the spectral resolution and the high scanning resolution allowed to realize a lifetime mapping of the diamond nanocluster, as depicted in Figure 8D. The integration for SNSPDs on a wavelength-discriminating on-chip circuitry allows to obtain a spectrally resolved single-photon detection with high timing precision in a single nanophotonic device.

The major limitations of AWG spectrometers are a limited number of channels and the need of very high yield for detectors and photonic circuitry components. Another solution is to use coherent detection techniques [249]. This method, successfully adopted for LiDAR and space applications, allows to obtain extremely high spectral resolution by using only one detector. The working principle, depicted in Figure 9A, B, consists of combining the signal of interest (S) with a weak local oscillator (LO). The

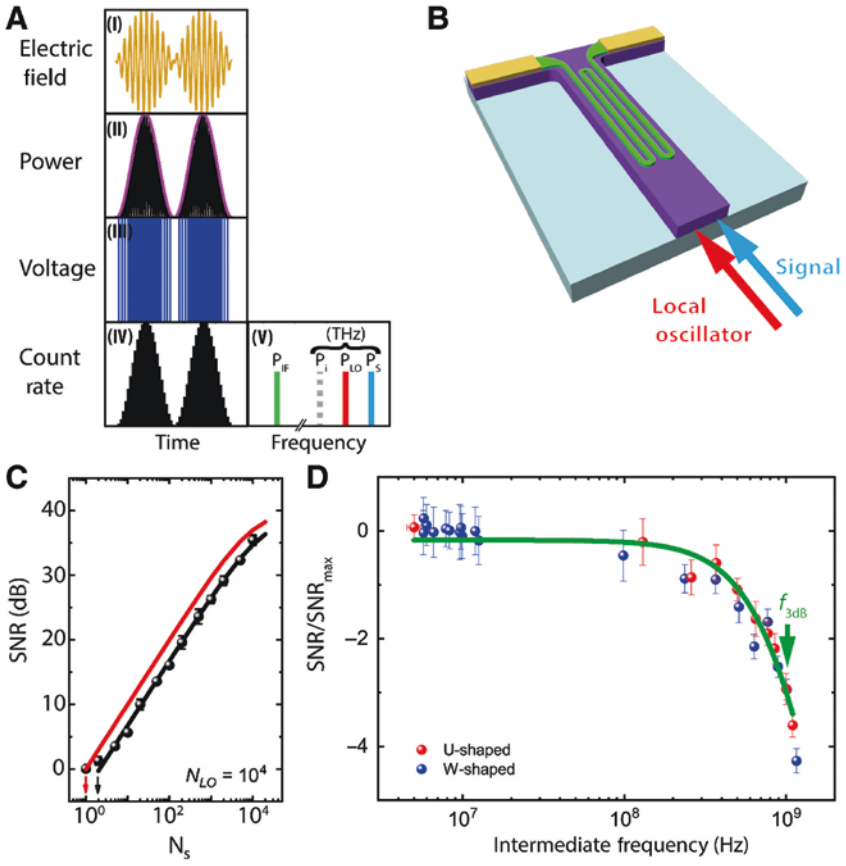

Figure 9: Heterodyne mixing with SNSPDs.
(A) (I) Time-domain beating of the EM field generated by the overlapping of the LO and the S fields with a slight frequency shift. (II) Power oscillation at the intermediate frequency. (III) Voltage response of the SNSPD in the presence of beating. (IV) Count rate as recorded by a frequency counter. (V) Detection response in the frequency domain. (B) Schematic view of the W-shape SNSPDs. (C) SNR at different signal photon flux. The red curve represents the response for an ideal shot-noise-limited photodetector, with unitary efficiency and no noise. The arrows indicate the minimum detectable signal for SNR = 0 dB. (D) Noise bandwidth for two different detectors geometries. The arrows indicate the −3 dB threshold used for the bandwidth determination. Figure adapted with permission from Ref. [245].

two signals start beating at an intermediate frequency (IF), which correspond to the signal and local oscillator frequency difference. By detecting the intermediate frequency and subtracting it from the known local oscillator frequency, it is possible to retrieve spectral information of the signal under investigation. This technique has been widely adopted in the past using hot electron bolometers [250]. The drawback of hot electron bolometers is that they exploit a thermal effect, which is slower, thus limiting the detection bandwidth. Solid-state single-photon detectors have been therefore introduced [251]. In this case, the response signal corresponds to a train of detection pulses, which repeat at the signals intermediate frequency. By adapting this technique with integrated SNSPDs, it is possible to exploit their extremely high speed to access a wider spectral bandwidth and their superior detection efficiency in the infrared range for an increased sensitivity. Coherent detection has been demonstrated using an 86% efficient waveguide-integrated SNSPD, with dark count rate of <100 cps at 80% of the switching current. To fully characterize the performance of this approach, two different experiments have been performed. The smallest detectable signal has been determined using a single CW laser source connected to a two-port fiber splitter, one of which was connected to an acousto-optic modulator for generating a local oscillator signal and test signal with a constant frequency shift of 400 MHz. The response signal of the detector has been amplified and analyzed using a spectrum analyzer (SA) to determine frequency and power of the beating signal. The minimal detectable power is limited by the SNR of the IF spectrum registered with the SA, which in turn depends on the detector efficiency (higher detection efficiency would allow to obtain a better SNR), dark count, electrical noise of the amplifiers and the dynamic range of the SNA. By controlling the local oscillator power, the SA resolution bandwidth and the

acquisition time, an ultimate sensitivity limit of roughly two times the photon energy has been obtained. In Figure 9C, we showed a comparison of the minimal detectable signal at different signal photon fluxes in comparison with the MDS for a shot-noise limited system (unitary detection efficiency and no dark counts). Quantum sensitivity can be potentially achieved with better efficient detectors and with improved low noise electronics. To determine the detection bandwidth, two different attenuated lasers, one acting a signal and a second, as local oscillator, were adopted. The measurement results are depicted in Figure 9D. The detection bandwidth is defined as the intermediate frequency value at which the SNR is reduced by 3 dB. The detection bandwidth was mainly limited by the bandwidth of the readout scheme, in particular, by the adopted room-temperature amplifiers. Spectral resolution at the single-photon level is of great interest for both classical and quantum optics. Coherent detection with integrated SNSPDs allows to achieve extremely sensitive spectroscopy with high resolution ($\Delta f/f > 10^{11}$). This technique can find interesting application for characterizing the emission spectra of on-chip sources, for communication multiplexing and for the investigation of extremely narrow fluorescence lines, also in the infrared region.

5 On-Chip characterization of single-photon sources

Quantum metrology and technology would benefit from the realization of on-chip structures containing single-photon sources, routing circuitry and detectors. Here we showcase three examples for the characterization of on-chip single-photon sources exploiting SNSPDs. In the first paragraph, time-resolved lifetime and second-order correlation of a quantum dot single-photon emission is presented. The second paragraph is dedicated to the realization of on-chip correlators for investigating the quantum Nature of integrated light sources.

5.1 On-chip time resolved detection of quantum dot emission

Solid-state emitters, such as in GaAs quantum dots (QDs), have been proposed as reliable and potentially scalable sources of single photon. These devices can be integrated with state-of-art GaAs photonic platform, which is compatible with the integration of superconducting nanowire single-photon detectors, as described in Section 3.1.3. Although electrically driven emission has been demonstrated [252, 253], optical excitation still represents the most effective method for single-photon generation using QDs. The main drawback of this technique is the need for filtering the excitation laser light, which is scattered through the substrate or coupled into the waveguide, thus reducing the SNR at the SNSPDs. Reithmaier et al. [166] overcame this limitation by temporally filtering the detector signal to recover the emission of self-assembled InGaAs quantum dots embedded in GaAs on AlGaAs waveguide with *in situ* detection, using a waveguide-integrated NbN SNSPD. As depicted in Figure 10A, a pulsed laser diode was used to excite the QD emission, which

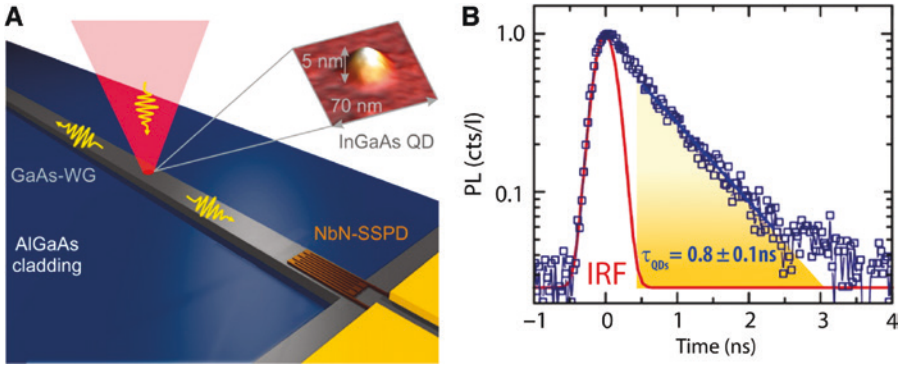

Figure 10: Integrated characterization of QD single photon emitters.
(A) Schematic of the on-chip structure consisting of a 2-mm-long GaAs ridge waveguide containing a single layer of InGaAs QDs. The QDs are excited by a free-space pulsed laser diode, and their emission coupled to the waveguide and propagated to the NbN detector. The inset reports an AFM scan of the QD. (B) Photoluminescence signal detected by the SNSPD. Units are in counts per detected laser photon (cts/l). In the absence of the quantum dot (red curve), the instrument response function (IRS) of the excitation laser is recorded. In the presence of the QDs (blue data points), an asymmetric behavior is observed. By subtracting the IRF, the QD emission lifetime can be determined. The yellow-shaded area indicates the integration window in which the QD lifetime has been extracted. Figure adapted with permission from [166] © American Chemical Society.

propagates through the GaAs waveguide and is detected by SNSPDs at a distance of 1040 ± 1 μm. QDs with sharp emission line were pre-selected using a confocal microscopy technique. In this experiment, the excitation laser was not filtered. An amorphous Si absorber layer has been deposited on the back surface of the chip to reduce the contribution of the stray light, and the luminescence signal has been retrieved by deconvolving the detector response signal and the excitation laser signal, using temporal filtering of the SNSPD response. The experimental results are reported in Figure 10B. In the absence of QDs, the time-resolved SNSPDs signal response function shows a Gaussian profile with FWHM of 290 ± 70 ps, reproducing the pulsed emission of the excitation laser. In the presence of a quantum dot, instead, an exponential decay of the response function is clearly visible. The decay rate has been determined to be $\tau_{QD} = (0.80 \pm 0.07)$ ns and is compatible with the InGaAs lifetime [254, 255]. An important advance using this technique is the characterization of the emission lifetime with SNSPDs without any filtering of the excitation light. An off-chip confocal characterization of the source's second order correlation function $g(2) = 0.36$ simultaneous to the on-chip fluorescence characterization confirms the single-photon Nature of the QDs photoluminescent signal characterized using the on-chip detectors. The high timing resolution of SNSPDs allows to characterize the emission lifetime of single-photon sources integrated onto an optical waveguide using a time-filtering technique, which does not require any kind of off-chip filter stage, which would inevitably reduce the emitted signal intensity. The main limitation is the system jitter and the time duration of the excitation pulse, which could, for short-lifetime sources, affect the discrimination of the source fluorescence decaying signal. These limitations could be overcome with an improvement of the readout electronics and, where possible, a reduction of the excitation pulse duration.

5.2 Integrated autocorrelator

One key functionality for the advancement of integrated quantum photonics is the ability of characterizing the classical and quantum Nature of on-chip light sources. Superconducting detectors represent an ideal solution to realize on-chip measurement of sources' second-order correlation with very low timing uncertainty. A very compact integrated autocorrelator has been proposed by Sahin et al. [256]. The scheme, depicted in the inset of Figure 11A, consists of two NbN SNSPDs (D1 and D2) integrated on top

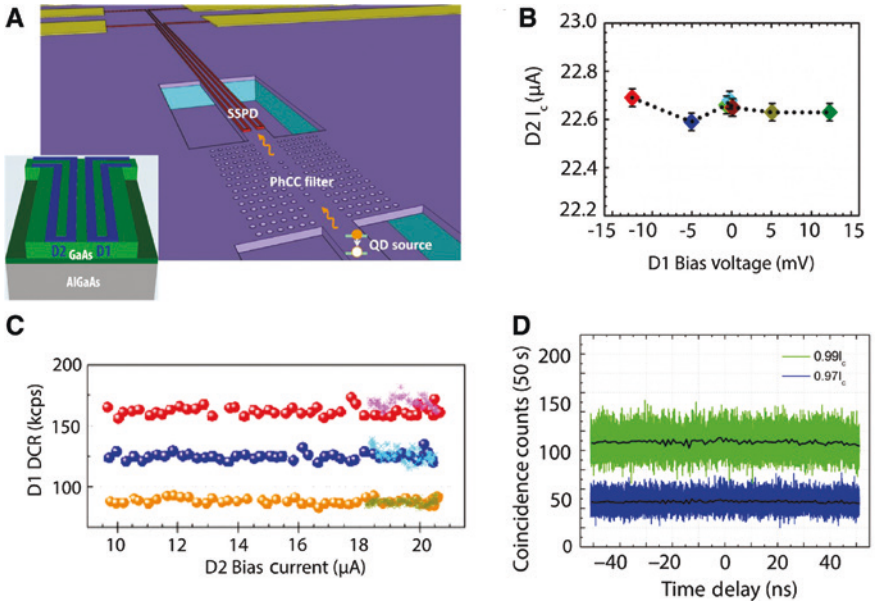

Figure 11: Integrated HBT measurement with SNSPDs.
(A) Schematic of the on-chip HBT experiment as proposed in Ref. [167]. The sketch in the inset represents the waveguide-integrated autocorrelator using two nanowires onto a photonic waveguide. (B) Influence of the bias voltage applied on the detector D1 on the critical current of the detector D2. Within the experimental accuracy, no cross-influence between the two structures has been observed. (C) Dark count rate of the detector D1 versus D2 bias current. Also, when D2 was in normal state (starred points), no influence on the DCR of the first detector has been observed. (D) Intensity autocorrelation for a CW laser measured with the integrated autocorrelator. The absence of artifacts within the measurement uncertainty allows to exclude dynamic cross talk between the two detectors. Figure adapted with permission from [167, 256] © OSA Publishing.

of the same GaAs waveguide. The main requirement for this design is symmetrical arrangement of the nanowires on the same waveguide to ensure equal coupling with the propagating evanescent field. The waveguide structure made of 300-nm GaAs on AlGaAs 1.85-μm wide was able to support both TE and TM modes, thus making the correlator polarization independent. Despite a calculated high absorption efficiency (>93%), the practical limitation of the system was low OCDE, related to a non-optimized film thickness, which compromised the internal quantum efficiency of the devices. This limitation can be overcome by improving the quality of the superconducting film. Importantly, the two detectors showed almost no cross-talk, resulting in a low noise system. Static cross-talk has been tested by measuring the variation of the switching current of one detector at different biasing conditions of the second detector (Figure 11B). In addition, a negligible contribution of the dark counts of one detector at different biasing to the second detector, as depicted in Figure 11C, has been shown. Better heat transport due to high thermal conductivity of GaAs could explain the reason for such low static cross-talk when compared with sapphire. The dynamic cross-talk, defined as the temporal variation of the detection probability of one detector due to switching of the second detector, has been tested by measuring the second-order autocorrelation function of a CW coherent light source (laser) and of a pulsed laser. As shown in Figure 11D, no artifacts in the coincidence counting signal have been found, confirming the absence of dynamic cross-talk. Uncertainty in propagation demonstrated a 4% experimental accuracy. Thicker superconducting film ensured high critical currents (22 μA), which are beneficial for a lower electronic SNR. The overall system jitter, using room-temperature amplifiers, has been determined to be 125 ps, near the switching current, which is sufficient for characterizing quantum dot single-photon emission. This very compact autocorrelator is a ready tool that can be adopted for the characterization of on-chip sources. A full architecture combining this autocorrelator with photoluminescent quantum dot sources and a photonic crystal cavity for on-chip filtering of the pump light is shown in Figure 11A. This structure has been successfully used to perform a TRPL characterization. The low extinction ratio of the pump light filtering block represents the main limiting factor. By placing the excitation spot far enough from the detector (500 μm or more), most of the signal was suppressed and only the QD emission was measured [167]. Evaluating the cross-talk for other substrates than GaAs would allow to adopt such a geometry also for different platforms. With an improved pump suppression, the proposed method is a convincing scheme, which could become a universal tool for fully integrated second-order autocorrelation measurement.

5.3 Fully integrated quantum photonic circuit with an electrically driven light source

Substantial research efforts are today dedicated on finding reliable and fast sources that can be easily integrated on a wafer scale and can be coupled to waveguiding structures [257]. High brightness, reproducibility and no blinking are not the only requirements for on-chip light sources. Two major challenges must be faced: efficient coupling to photonic waveguides and the possibility of directly exploiting the emitted light on chip. Different solutions like quantum dots [166, 258], color centers [203] and parametric down conversion in nonlinear materials [162] have been proposed. External light can be easily coupled to waveguides or, in the case of nonlinear effects, can be directly generated inside the waveguiding material. On the other hand, a major bottleneck in the application of these sources for a full on-chip architecture is that these sources require optical excitation with light, which needs to be filtered on chip with very high extinction ratio. The pump light is typically orders of magnitude more intense than the emitted light, and on-chip filters capable of fully suppressing this undesired contribution are challenging to implement. Furthermore, integrated filters are generally based on waveguiding structures generating thermal effects and reflection, negatively influencing the functionality of the routing and detection components of the system. Therefore, in many of the experiments, light is filtered off-chip with a subsequent degradation of the original signal. A desirable solution is offered by adopting electrically driven single-photon sources, which do not need of any kind of external optical excitation. As proof of principle of a full on-chip source characterization experiment, a second-order correlation measurement of a carbon nanotube-based electrically driven single-photon source was performed [160]. Single-walled semiconducting carbon nanotubes (sc-SWCNTs) can operate at low temperatures and can also be deposited on a large scale using dielectrophoresis [259]. The nanotubes emission wavelength can be chosen by chirality and diameter and can span from the visible to the NIR wavelengths [260]. Furthermore, high emission rates on the order of Gcps have been reported [261], with would enable ultra-fast on-chip quantum optic processing. To characterize the quantum Nature of the waveguide-coupled light source, a fully integrated architecture for

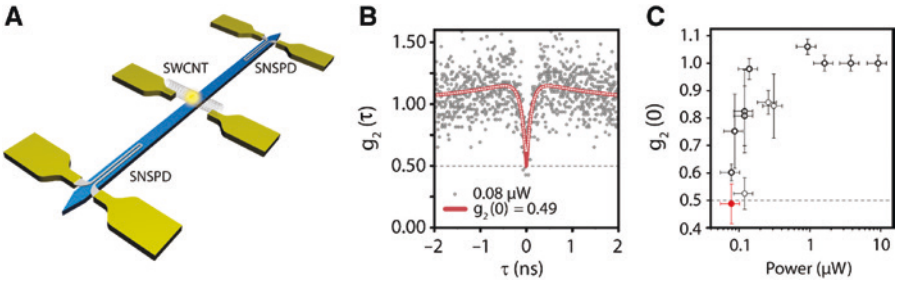

Figure 12: On-chip characterization of CNT single photon emitters.
(A) Schematic view of the on-chip device. The electrically stimulated emission from a sc-SWCNT couples and propagates inside the waveguide and reaches the integrated detectors. Due to the chirality properties of the emitter, the symmetric configuration allows 50:50 splitting of the emitted photons among the two detectors. (B) Coincidence histogram of non-classical light emission from the electrically driven nanotube obtained with the integrated correlator. (C) Zero-delay correlation function for different electrical power applied to the carbon nanotube. Figure adapted with permission from [160] © Springer Nature.

Hanbury-Brown-Twiss experiment has been realized. The system geometry, depicted in Figure 12A, consists of two waveguides integrated SNSPDs symmetrically located at the opposite side of a SiN waveguide on which a sc-SWCNT has been deposited. The whole characterization has been performed at exchange gas temperature of 1.6 K, using a liquid-helium cryostat. The emitted light evanescently couples to the waveguide and propagates towards the nanowire. Because of the symmetric position of the detectors with respect to the emission point, the waveguide acts as a beam splitter. By correlating the count rates of the detectors for different electrical excitation powers, antibunching characteristics of the source shown in Figure 12B could be observed. A limitation of this experiment was the short lifetime of the source (~72 ps), which is close to the system timing uncertainty. The system jitter was in fact limited by the readout electronics. By improving the electronics, using, for instance, cryogenic amplifier, better performance can be reached. In addition, it is important to consider that the whole experiment has been performed by driving the source with continuous current. The visibility could be improved by adjusting the excitation electronics for pulsed excitation. The experiment represents a successful demonstration of the integration of superconducting nanowire single-photon detectors for a full on-chip characterization of single-photon sources. The same architecture can be potentially adopted for any waveguide coupled source that does not need optical excitation. As a further improvement, a very interesting architecture for the simultaneous, full characterization of a single-photon state has been recently proposed by Thomay et al. [262]. Although demonstrated for stand-alone sources and detectors, this method can be adopted for a fully integrated on-chip cross correlation measurement using four single-photon detectors. This would represent a very fast and accurate way to fully characterize a single-photon source, with existing integrated technology and detectors.

6 On-chip quantum interference

Next, the application of nanophotonic-embedded SNSPDs for quantum interference experiments will be presented. In the first paragraph, on-chip photon interference and detection have been realized on a silicon platform, while in the second paragraph, SNSPDs have been adopted to characterize on-chip plasmon interference.

6.1 On-chip quantum interference

Quantum interference is of fundamental importance for exploring the quantum Nature of light and for quantum processing. This effect has been experimentally observed by Hong, Ou and Mandel (HOM) in 1987 [263]. When two indistinguishable single-photon reach a beam splitter simultaneously, they will interfere non-classically. They will be both reflected or transmitted through the beam splitter; therefore, the probability that the two photons will leave the beam splitter separately is zero. By modifying the path difference between the two photons and collecting the coincidence of the arrival of the photons at the two branches of the beam splitter with two single-photon detectors, it is possible to observe a dip in the coincidence probability at the zero-delay arrival time. This is the so-called HOM dip and is a clear sign of single photon's indistinguishability. The width of the dip is given by the photons coherence time, while the depth indicates the

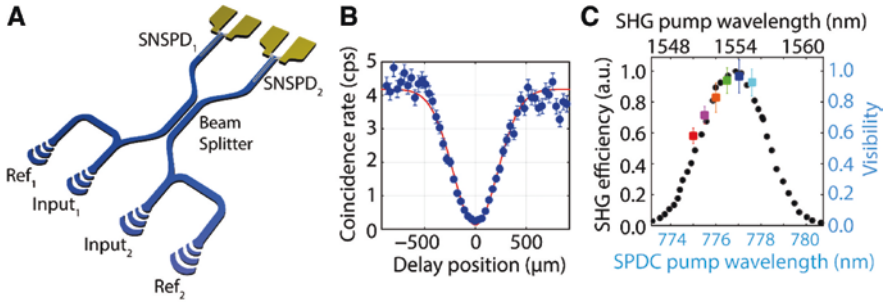

Figure 13: On-chip quantum interference.
(A) Schematic of the on-chip interferometer. Two input focusing grating couplers are used to inject the photon pairs in the circuit. An external delay line is used to scan the arrival time of the photons at the beam splitter. Two reference ports (Ref_1, Ref_2) are used to control the input photon flux. The beam splitter consists of a directional coupler, which length has been optimized to maximize the photon pair mode overlap. SNSPDs are allocated at each output of the beam splitter for the coincidence measurement made with external coincidence electronics. (B) Coincidence detection rate between the two SNSPDs as function of the optical delay line position. The nominal pump power of the SPDC was set to 10.5 mW. (C) HOM interference visibility as a function of the SPDC pump wavelength (colored symbols). Black symbols represent the SHG efficiency as a function of the pump wavelength for the ppKTP crystal. Figure adapted with permission from [149].

level suppression of the photons coincidence probability, which is called visibility and expresses the purity of the single-photon state. Linear optics quantum computation is based on quantum interference of multiple photons [46, 48, 49, 264]. Integrated optics offers a complete set of ready-to-use building blocks such as beam splitters, interferometers and phase shifters for implementing quantum operators. The basic architecture for HOM interference consists of a single-photon source, a tunable delay line, a beam splitter and two single-photon detectors. On-chip quantum interference has been realized on SiN on SiO_2 substrate using a directional coupler device, acting as a beam splitter, and two NbTiN superconducting nanowire single-photon detectors, as depicted in Figure 13A [149]. An important advantage of this on-chip application is that the spatial overlap between the input modes of the directional coupler is guaranteed by the high lithographic control over the waveguide dimensions. For this experiment, an off-chip spontaneous parametric down conversion source (SPDC), a periodically poled potassium titanyl phosphate (ppKTP) crystal waveguide, has been used. The source was excited with a 775-nm pump laser to generate photon pairs at 1550 nm. The pump signal has been suppressed by using a 1064-nm long pass and a 1550-nm band pass filter. After adjusting the polarization of the emitted photons and the temporal delay between the two photons by the mean of an optical delay line, the photon pair has been transmitted into an on-chip interferometer at a temperature of 1.7 K. The coupling between the source and the on-chip interferometer has been performed using different conversion stages from free space, to fiber to grating couplers resulting in high coupling losses. Thanks to the extremely high SNR of superconducting nanowire single-photon detectors, by scanning the delay line around the zero-path difference, it has been possible to observe HOM interference with 97% visibility, as shown in Figure 13B. In Figure 13C, the dependence of the interfering single-photon state purity on the pump laser wavelength was presented. A degradation of the visibility by detuning the pump laser out of the quasi phase matching condition can be observed. More compact photonic structures, such as multimode interference (MMI) devices, can be adopted for the realization of an on-chip interferometer [265]. These structures do not only provide smaller footprint but also allow a more robust control in fabrication, allowing to maximize the spatial overlap between the interacting modes.

6.2 Quantum interference in plasmonic circuits

When many functional devices on a single chip are needed, small footprint becomes very important. Dielectric waveguides are diffraction-limited systems, and the device size is still very large when compared with integrated electronics. Exploiting surface plasmon polaritons, which can propagate in extremely confined structures, allows to beat the diffraction limitation. SNSPDs have been demonstrated to be suitable also for the detection of single surface plasmon polaritons [266]. Single-photon impinging on a plasmonic waveguide has been used to excite plasmons, which propagate through a 7.5-μm waveguide equipped with NbN nanowires. A correlation measurement between off-chip APDs used to characterize the single-photon source emission and the on-chip detectors employed to count the plasmons propagating within the on-chip plasmonic waveguide allowed to confirm

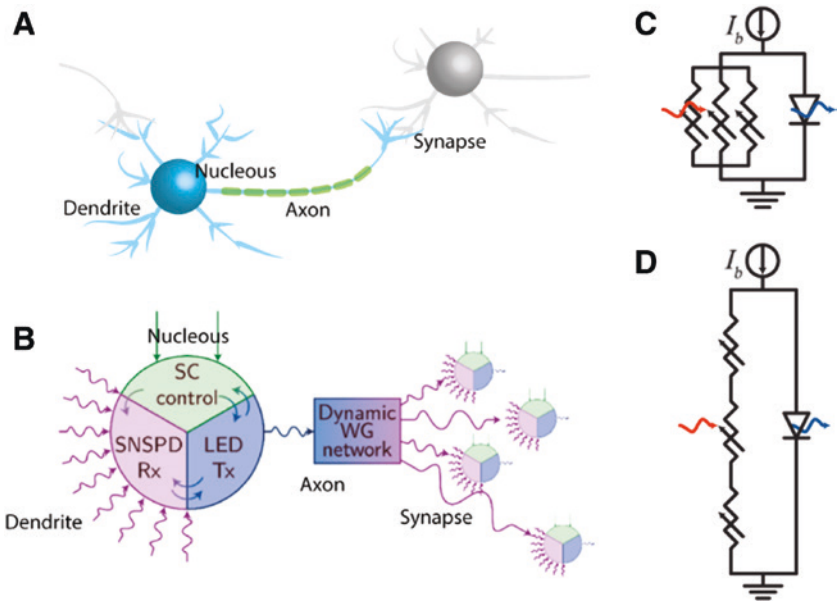

Figure 14: Neuromorphic computing with SNSPDs.
(A) Simplified scheme of a neuron. (B) Hybrid nanophotonic and superconducting scheme for neuron mimic. SNSPDs serve as dendrites for the reception of a synaptic signal. Superconducting electronics (SC) controls the signal, and when a threshold is reached, the LED transmits a new light pulse (synapse) that can propagate to the adjacent unit or fan out inside the waveguide network. (C) PND neuron circuit. A detection event in one or more SNSPDs, here depicted as variable resistors, drives the bias current to the parallel LED. When the lasing threshold is reached, a light burst is emitted. (D) SND neuron circuit. Photon absorption in long SNSPDs, depicted as a series of many resistors, generates sections with normal state resistance. With the increase of the absorbed photons, many more sections are switched to the normal state, causing an increase of the LED voltage, producing an optical signal. Figure adapted with permission from [268] © American Physical Society.

the original photons counting statistics, thus confirming single plasmon sensitivity of the system. In addition, Heeres et al. [267] showed quantum interference between indistinguishable plasmons using plasmonic-waveguide integrated NbN SNSPDs. This representative experiment paves the way for a smaller sized integrated platform for quantum information processing. Single photon generated by a type II SPDC source has been separated into two channels and coupled to different inputs of a two-port plasmonic beam splitter. The polarization of the two channels has been optimized to maximize the plasmon excitation. The beam splitter output was directed to two NbN superconducting meander-shaped nanowires made of a 5-nm-thick and 100-nm-wide NbN strip. By adjusting the time delay between the excitation photons and thus the arrival time of the two polaritons at the beam splitter, it was possible to observe the Hong-Ou-Mandel (HOM) dip at zero-time delay with a best-case visibility of 0.43 ± 0.02. Further analysis and simulation allowed the authors to confirm that the reduced visibility compared to the one observed with the generated photon pairs of 0.92 ± 0.01 can be associated with the excitation of long-range surface plasmons, which are not strongly confined. Supplementary simulation hinted an imperfect mode overlap in the beam splitter, which resulted in a reduction of visibility by 8%. An analysis of the time-resolved correlation allowed to determine a coherence time of 2.49 ± 0.08 ps, very similar to the coherence time of the single-photon pair (2.51 ± 0.03 ps), confirming that the plasmonic mode propagation does not degrade the wave-packed temporal resolution. This first experiment of quantum interference between surface plasmon polaritons on a chip opens new possibilities for compact quantum optics not limited by the conventional diffraction size, with potential to push towards the length scale of electronic components.

7 Superconducting detectors for neuromorphic computing

Advancement in artificial intelligence and machine learning for big data analysis, smart stock trades and autonomous vehicles applications created a growing interest in the potential offered by neuromorphic computing. The aim is to realize systems capable of mimicking the functionality of the human brain by reproducing neuron functionality and the generation of synapses.

In a very simplified scheme, as depicted in Figure 14A, B, a neuronal unit is composed of a dendritic harbor, a nucleous and an a synaptic terminal (axon) [269]. The dendric harbor is responsible for receiving signals from other neurons. The nucleous is responsible for establishing whether the incoming signals can propagate towards other cells or not (integration function), and depending on the neuron functionality, if a certain threshold is overcome, a pulse will be sent to an adjacent neuron or fan out to many more neurons (synapses) through the axon. Considering that, in a human brain, 10^{11} neurons with 10^{14} synapses are present, the requirement for massive scalability and low power consumption carries significant weight for a feasible artificial brain system.

To satisfy the requirement for energy-efficient interconnection of a large number of processing units (neurons), photonics has been proposed as a platform for the realization of tailored hardware for neuromorphic computing [270]. The non-interacting Nature of photons would allow manifold interconnections, thus overcoming the parasitic cross-talk limitation of electronic components. Furthermore, in the optical domain, more degrees of freedom such as polarization, frequency and photon number can be exploited and small footprint optical interconnectivity among different neurons can be obtained with integrated nanophotonic waveguides. SNSPDs represent an attractive choice for this application to realize spiking neural communication, where interconnected units transmit information through pulses or bursts of pulses. Because of their sensitivity, single-photon would potentially be capable of triggering spiking events with high energy efficiency.

The adoption of integrated optical devices including SNSPDs has recently been proposed by Shainline et al. [268] with two different schemes. In the first scheme, as depicted in Figure 14C, an integrated and fire threshold unit has been realized using a parallel nanowire detector (PND) in which many nanowire detectors are connected in parallel to an on-chip faint-light light emitting diode with high impedance. In steady state, the supercurrent will flow in the detector branch and, because of its high impedance, almost no current flows on the LED and no photon spike are emitted. The threshold level is set by opportunely designing the number of the nanowires in the parallel configuration. Input light excitation is multiplexed through the different detectors, and only if a sufficient number of detectors switch to the normal state that the bias current is diverted to the LED and generates an optical spike. The spike duration depends on the detectors' recovery time and the lifetime of the LED emitter. Considering the extremely short recovery time of SNSPDs, currently, the latter contribution represents the main limitation for the neural network communication rate. A second configuration, shown in Figure 14D, where a long nanowire made from a series of nanowire detectors (SND), in parallel to the LED emitter, is capable of generating a continuous response has also been proposed. Such a scheme is important for implementing neural back propagation algorithms [271].

To build a neural network, high-yield devices are needed. WSi detectors have been demonstrated to be very promising in this regard, and the realization of Si p-i-n junction on a Si platform has been shown to provide very efficient emitters, which can operate at low temperatures and can easily be coupled with a Si nanophotonic platform. To realize thousands of units and interconnections with low loss and low cross-talk, three-dimensional photonic schemes have also been proposed by stacking waveguides [272]. Another important requirement for mimicking the human brain is synaptic weighting [273, 274], i.e. the increase of the strain of particular synapses depending on their usage. Nanophotonics offers ready building blocks for this application, such as electro-mechanical waveguide couplers [275] or electro-absorption modulators [276].

8 Conclusion and outlook

Exploring new materials and new platforms would allow to retrieve more information about the physics underlying the detection mechanism, which could in turn unlock new functionalities and improvements of performance metrics. Exploring small superconducting gap materials, for instance, would allow to extend the detector sensitivity to longer wavelengths and to achieve high internal quantum efficiency also at low bias currents. Research interest should also focus on new photonic platforms for detectors integration, with the aim to functionalize the thermalization processes that control the detection dynamics, thus reducing their latency time. In addition, the development of custom electronics to optimally harness the superior performance metrics of SNSPDs is of high importance, including counting electronics, and also low-temperature electronics for devices readout, in particular, for achieving a further reduction of the timing jitter of these detectors and a higher maximum count rate. Significant efforts should also be invested on finding more efficient approaches for interfacing these detectors with external circuitry, thus allowing more efficient chip-to-chip communication. As one of the weak points for SNSPDs application is the need of relatively low cryogenic temperatures, high-Tc superconducting materials, which can be easily integrated on

nanophotonics circuitry, would allow to use more compact and affordable cryogenic equipment. Use of SNSPDs for neural network applications is a demonstration that these devices can find applications in fields that go beyond the pure detection of single photon. This confirms that waveguide-integrated superconducting nanowire single-photon detectors are and will be also essential components in the future for the advance of optical quantum technology, on-chip computation and life Science applications.

Acknowledgments: C.S. acknowledges financial support from the Ministerium für Innovation, Wissenschaft und Forschung des Landes Nordrhein-Westfalen. We acknowledge support by the Open Access Publication Fund of the University of Muenster.

Funding: European Research Council, Funder Id: http://dx.doi.org/10.13039/501100000781, Grant Number: 724707; Volkswagen Foundation, Grant Name WINS PINQS.

References

[1] Koenderink AF, Alù A, Polman A. Nanophotonics: shrinking light-based technology. Science 2015;348:516–21.
[2] Thomson D, Zilkie A, Bowers JE, et al. Roadmap on silicon photonics. J Opt 2016;18:073003.
[3] Silverstone JW, Bonneau D, O'Brien JL, Thompson MG. Silicon quantum photonics. IEEE J Sel Top Quantum Electron 2016;22:390–402.
[4] O'Brien JL. Optical quantum computing. Science 2007;318:1567–70.
[5] Politi A, Matthews JCF, Thompson MG, O'Brien JL. Integrated quantum photonics. IEEE J Sel Top Quantum Electron 2009;15:1673–84.
[6] O'Brien JL, Furusawa A, Vučković J. Photonic quantum technologies. Nat Photonics 2009;3:687–95.
[7] Dietrich CP, Fiore A, Thompson MG, Kamp M, Höfling S. GaAs integrated quantum photonics: towards compact and multi-functional quantum photonic integrated circuits. Laser Photonics Rev 2016;10:870–94.
[8] Eisaman MD, Fan J, Migdall A, Polyakov SV. Invited review article: single-photon sources and detectors. Rev Sci Instrum 2011;82:071101.
[9] Photomultiplier tubes: basics and applications, 3a ed. Hamamatsu, 2007.
[10] Razeghi M. Single-photon avalanche photodiodes, in technology of quantum devices. Boston, MA, Springer, 2010, 425–55.
[11] Cova S, Ghioni M, Lacaita A, Samori C, Zappa F. Avalanche photodiodes and quenching circuits for single-photon detection. Appl Opt 1996;35:1956–76.
[12] Kim J, McKay KS, Stapelbroek MG, Hogue HH. Opportunities for single-photon detection using visible light photon counters. in Advanced Photon Counting Techniques V 2011;8033:80330Q.
[13] Hadfield RH, Johansson G. Eds. Superconducting devices in quantum optics. Berlin, Springer International Publishing, 2016.
[14] Rosenberg D, Lita AE, Miller AJ, Nam SW. Noise-free high-efficiency photon-number-resolving detectors. Phys Rev A 2005;71:061803.
[15] Natarajan CM, Tanner MG, Hadfield RH. Superconducting nanowire single-photon detectors: physics and applications. Supercond Sci Technol 2012;25:063001.
[16] Ferrari S, Kovalyuk V, Hartmann W, et al. Hot-spot relaxation time current dependence in niobium nitride waveguide-integrated superconducting nanowire single-photon detectors. Opt Express 2017;25:8739–50.
[17] Engel A, Renema JJ, Il'in K, Semenov A. Detection mechanism of superconducting nanowire single-photon detectors. Supercond Sci Technol 2015;28:114003.
[18] Vodolazov DY. Single-photon detection by a dirty current-carrying superconducting strip based on the kinetic-equation approach. Phys Rev Appl 2017;7:034014.
[19] Lusche R, Semenov A, Huebers H-W, et al. Effect of the wire width on the intrinsic detection efficiency of superconducting-nanowire single-photon detectors. J Appl Phys 2014;116:043906.
[20] Hofherr M, Rall D, Ilin K, et al. Intrinsic detection efficiency of superconducting nanowire single-photon detectors with different thicknesses. J Appl Phys 2010;108:014507.
[21] Kerman AJ, Dauler EA, Keicher WE, et al. Kinetic-inductance-limited reset time of superconducting nanowire photon counters. Appl Phys Lett 2006;88:111116.
[22] Sidorova M, Semenov A, Hubers H-W, et al. Physical mechanisms of timing jitter in photon detection by current-carrying superconducting nanowires. Phys Rev B 2017;96:184504.
[23] Heeres RW, Zwiller V. Superconducting detector dynamics studied by quantum pump-probe spectroscopy. Appl Phys Lett 2012;101:112603.
[24] Marsili F, Stevens MJ, Kozorezov A, et al. Hotspot relaxation dynamics in a current-carrying superconductor. Phys Rev B 2016;93:094518.
[25] Renema JJ, Gaudio R, Wang Q, et al. Experimental test of theories of the detection mechanism in a nanowire superconducting single photon detector. Phys Rev Lett 2014;112:117604.
[26] Renema JJ, Gaudio R, Wang Q, et al. Probing the hotspot interaction length in NbN nanowire superconducting single photon detectors. Appl Phys Lett 2017;110:233103.
[27] Semenov AD, Haas P, Günther B, Hübers H-W, Il'in K, Siegel M. Energy resolution of a superconducting nanowire single-photon detector. J Low Temp Phys 2008;151:564–9.
[28] Lusche R, Semenov A, Korneeva Y, et al. Effect of magnetic field on the photon detection in thin superconducting meander structures. Phys Rev B 2014;89:104513.
[29] Kozorezov AG, Lambert C, Marsili F, et al. Quasiparticle recombination in hotspots in superconducting current-carrying nanowires. Phys Rev B 2015;92:064504.
[30] Gol'tsman GN, Okunev O, Chulkova G, et al. Picosecond superconducting single-photon optical detector. Appl Phys Lett 2001;79:705–7.
[31] Kadin AM, Johnson MW. Nonequilibrium photon-induced hotspot: a new mechanism for photodetection in ultrathin metallic films. Appl Phys Lett 1996;69:3938–40.
[32] Semenov AD, Gol'tsman GN, Korneev AA. Quantum detection by current carrying superconducting film. Phys C Supercond 2001;351:349–56.
[33] Semenov A, Engel A, Il'in K, Gol'tsman G, Siegel M, Hübers H-W. Ultimate performance of a superconducting quantum detector. Eur Phys J Appl Phys 2003;21:171–8.

[34] Semenov A, Engel A, Hübers H-W, Il'in K, Siegel M. Spectral cut-off in the efficiency of the resistive state formation caused by absorption of a single-photon in current-carrying superconducting nano-strips. Eur Phys B – Condens Matter Complex Syst 2005;47:495–501.
[35] Engel A, Schilling A. Numerical analysis of detection-mechanism models of superconducting nanowire single-photon detector. J Appl Phys 2013;114:214501.
[36] Zotova AN, Vodolazov DY. Photon detection by current-carrying superconducting film: a time-dependent Ginzburg-Landau approach. Phys Rev B 2012;85:024509.
[37] Bulaevskii LN, Graf MJ, Batista CD, Kogan VG. Vortex-induced dissipation in narrow current-biased thin-film superconducting strips. Phys Rev B 2011;83:144526.
[38] Engel A, Lonsky J, Zhang X, Schilling A. Detection mechanism in SNSPD: numerical results of a conceptually simple, yet powerful detection model. IEEE Trans Appl Supercond 2015;25:1–7.
[39] Bulaevskii LN, Graf MJ, Kogan VG. Vortex-assisted photon counts and their magnetic field dependence in single-photon superconducting detectors. Phys Rev B 2012;85:014505.
[40] Kozorezov AG, Lambert C, Marsili F, et al. Fano fluctuations in superconducting-nanowire single-photon detectors. Phys Rev B 2017;96:054507.
[41] Annunziata AJ, Quaranta O, Santavicca DF, et al. Reset dynamics and latching in niobium superconducting nanowire single-photon detectors. J Appl Phys 2010;108:084507.
[42] Kerman AJ, Yang JKW, Molnar RJ, Dauler EA, Berggren KK. Electrothermal feedback in superconducting nanowire single-photon detectors. Phys Rev B 2009;79:100509.
[43] Feynman RP. Feynman lectures on physics. Volume 2: mainly electromagnetism and matter. 1964.
[44] Dauler EA, Grein ME, Kerman AJ, et al. Review of superconducting nanowire single-photon detector system design options and demonstrated performance. Opt Eng 2014;53:081907.
[45] Hadfield RH. Single-photon detectors for optical quantum information applications. Nat Photonics 2009;3:696–705.
[46] Knill E, Laflamme R, Milburn GJ. A scheme for efficient quantum computation with linear optics. Nature 2001;409:46.
[47] Varnava M, Browne DE, Rudolph T. How good must single photon sources and detectors be for efficient linear optical quantum computation? Phys Rev Lett 2008;100:060502.
[48] Spring JB, Metcalf BJ, Humphreys PC, et al. Boson sampling on a photonic chip. Science 2013;339:798–801.
[49] Tillmann M, Dakić B, Heilmann R, Nolte S, Szameit A, Walther P. Experimental boson sampling. Nat Photonics 2013;7:540.
[50] Wang H, He Y, Li Y-H, et al. High-efficiency multiphoton boson sampling. Nat Photonics 2017;11:361–5.
[51] Carolan J, Harrold C, Sparrow C, et al. Universal linear optics. Science 2015;349:711–6.
[52] Valivarthi R, Puigibert MG, Zhou Q, et al. Quantum teleportation across a metropolitan fibre network. Nat Photonics 2016;10:676–80.
[53] Xu P, Yong HL, Chen LK, et al. Two-hierarchy entanglement swapping for a linear optical quantum repeater. Phys Rev Lett 2017;119:170502.
[54] Sibson P, Kennard JE, Stanisic S, Erven C, O'Brien JL, Thompson MG. Integrated silicon photonics for high-speed quantum key distribution. Optica 2017;4:172–7.
[55] Liao S-K, Cai W-Q, Handsteiner J, et al. Satellite-relayed intercontinental quantum network. Phys Rev Lett 2018;120:030501.
[56] Diamanti E, Takesue H, Langrock C, Fejer MM, Yamamoto Y. 100 km differential phase shift quantum key distribution experiment with low jitter up-conversion detectors. Opt Express 2006;14:13073–82.
[57] Gisin N, Ribordy G, Tittel W, Zbinden H. Quantum cryptography. Rev Mod Phys 2002;74:145–95.
[58] Gisin N, Thew R. Quantum communication. Nat Photonics 2007;1:165–71.
[59] Wang X-L, Chen L-K, Li W, et al. Experimental ten-photon entanglement. Phys Rev Lett 2016;117:210502.
[60] Achilles D, Silberhorn C, Sliwa C, et al. Photon-number-resolving detection using time-multiplexing. J Mod Opt 2004;51:1499–515.
[61] Kaneda F, Christensen BG, Wong JJ, Park HS, McCusker KT, Kwiat PG. Time-multiplexed heralded single-photon source. Optica 2015;2:1010–3.
[62] Lee C, Ferrari S, Pernice WHP, Rockstuhl C. Sub-Poisson-binomial light. Phys Rev A 2016;94:053844.
[63] Raffaelli F, Ferranti G, Mahler DH, et al. A homodyne detector integrated onto a photonic chip for measuring quantum states and generating random numbers. Quantum Sci Technol 2018;3:025003.
[64] Zeilinger A. Light for the quantum. Entangled photons and their applications: a very personal perspective. Phys Scr 2017;92:072501.
[65] Tsujimoto Y, Sugiura Y, Tanaka M, et al. High visibility Hong-Ou-Mandel interference via a time-resolved coincidence measurement. Opt Express 2017;25:12069–80.
[66] Borst JW, Visser AJWG. Fluorescence lifetime imaging microscopy in life sciences. Meas Sci Technol 2010;21:102002.
[67] Gershanov S, Michowiz S, Toledano H, et al. Fluorescence lifetime imaging microscopy, a novel diagnostic tool for metastatic cell detection in the cerebrospinal fluid of children with medulloblastoma. Sci Rep 2017;7:3648.
[68] Yamashita T, Liu D, Miki S, et al. Fluorescence correlation spectroscopy with visible-wavelength superconducting nanowire single-photon detector. Opt Express 2014;22:28783–9.
[69] Wouters FS. The physics and biology of fluorescence microscopy in the life sciences. Contemp Phys 2006;47:239–55.
[70] Li L, Davis LM. Single photon avalanche diode for single molecule detection. Rev Sci Instrum 1993;64:1524–9.
[71] Stathis JH, Kastner MA. Time-resolved photoluminescence in amorphous silicon dioxide. Phys Rev B 1987;35:2972–9.
[72] Stevens MJ, Hadfield RH, Schwall RE, Nam SW, Mirin RP. Time-correlated single-photon counting with superconducting single-photon detectors. in Advanced Photon Counting Techniques 2006;6372:63720U.
[73] Gemmell NR, McCarthy A, Liu B, et al. Singlet oxygen luminescence detection with a fiber-coupled superconducting nanowire single-photon detector. Opt Express 2013;21:5005–13.
[74] Eraerds P, Legre M, Zhang J, Zbinden H, Gisin N. Photon counting OTDR: advantages and limitations. J Light Technol 2010;28:952–64.
[75] Schuck C, Pernice WHP, Ma X, Tang HX. Optical time domain reflectometry with low noise waveguide-coupled superconducting nanowire single-photon detectors. Appl Phys Lett 2013;102:191104.
[76] Wang S, Fan X, He Z. Ultrahigh resolution optical reflectometry based on linear optical sampling technique with digital dispersion compensation. IEEE Photonics J 2017;9:1–10.

[77] Priedhorsky WC, Smith RC, Ho C. Laser ranging and mapping with a photon-counting detector. Appl Opt 1996;35:441–52.
[78] Bao Z, Liang Y, Wang Z, et al. Laser ranging at few-photon level by photon-number-resolving detection. Appl Opt 2014;53:3908–12.
[79] Baek B, Stern JA, Nam SW. Superconducting nanowire single-photon detector in an optical cavity for front-side illumination. Appl Phys Lett 2009;95:191110.
[80] Dorenbos SN, Reiger EM, Akopian N, et al. Superconducting single photon detectors with minimized polarization dependence. Appl Phys Lett 2008;93:161102.
[81] Verma VB, Marsili F, Harrington S, Lita AE, Mirin RP, Nam SW. A three-dimensional, polarization-insensitive superconducting nanowire avalanche photodetector. Appl Phys Lett 2012;101:251114.
[82] Marsili F, Verma VB, Stern JA, et al. Detecting single infrared photons with 93% system efficiency. Nat Photonics 2013;7:210–4.
[83] Smirnov K, Divochiy A, Vakhtomin Y, et al. NbN single-photon detectors with saturated dependence of quantum efficiency. Supercond Sci Technol 2018;31:035011.
[84] Fiddy M. Fundamental Limits of Photon Detection (Detect) – DARPA-BAA-16-25 (Archived) – Federal Business Opportunities: Opportunities. [Online]. (Accessed January 17 2018, at https://www.fbo.gov/index?s=opportunity&mode=form&id=6d13cf57d50d88aeff23e77a0ca3d4ba&tab=core&_cview=0.)
[85] Microchannel plate photomultiplier tube R3809U-64. [Online]. (Accessed July 13, 2018, at https://www.hamamatsu.com/eu/en/product/type/R3809U-64/index.html.
[86] Thermoelectric cooled NIR-PMT unit H10330C | Hamamatsu Photonics. [Online]. (Accessed July 13, 2018, at https://www.hamamatsu.com/eu/en/product/type/H10330C/index.html.)
[87] Nevet A, Hayat A, Orenstein M. Ultrafast three-photon counting in a photomultiplier tube. Opt Lett 2011;36:725–7.
[88] Takeuchi S, Kim J, Yamamoto Y, Hogue HH. Development of a high-quantum-efficiency single-photon counting system. Appl Phys Lett 1999;74:1063–5.
[89] Kim J, Takeuchi S, Yamamoto Y, Hogue HH. Multiphoton detection using visible light photon counter. Appl Phys Lett 1999;74:902–4.
[90] Rech I, Labanca I, Armellini G, Gulinatti A, Ghioni M, Cova S. Operation of silicon single photon avalanche diodes at cryogenic temperature. Rev Sci Instrum 2007;78:063105.
[91] Liu M, Hu C, Bai X, et al. High-performance InGaAs/InP single-photon avalanche photodiode. IEEE J Sel Top Quantum Electron 2007;13:887–94.
[92] Dixon AR, Dynes JF, Yuan ZL, Sharpe AW, Bennett AJ, Shields AJ. Ultrashort dead time of photon-counting InGaAs avalanche photodiodes. Appl Phys Lett 2009;94:231113.
[93] Fukuda D, Fujii G, Yoshizawa A, et al. Titanium superconducting photon-number-resolving detector. IEEE Trans Appl Supercond 2011;21:241–5.
[94] Korzh BA, Zhao Q-Y, Frasca S, et al. Demonstrating sub-3 ps temporal resolution in a superconducting nanowire single-photon detector. ArXiv180406839 Cond-Mat Physicsphysics Physicsquant-Ph 2018.
[95] Langrock C, Diamanti E, Roussev RV, Yamamoto Y, Fejer MM, Takesue H. Highly efficient single-photon detection at communication wavelengths by use of upconversion in reverse-proton-exchanged periodically poled LiNbO3 waveguides. Opt Lett 2005;30:1725–7.
[96] Itzler MA, Ben-Michael R, Hsu C-F, et al. Single photon avalanche diodes (SPADs) for 1.5 μm photon counting applications. J Mod Opt 2007;54:283–304.
[97] Clem JR, Berggren KK. Geometry-dependent critical currents in superconducting nanocircuits. Phys Rev B 2011;84:174510.
[98] Henrich D, Reichensperger P, Hofherr M, et al. Geometry-induced reduction of the critical current in superconducting nanowires. Phys Rev B 2012;86:144504.
[99] Ilin K, Henrich D, Luck Y, Liang Y, Siegel M, Vodolazov DY. Critical current of Nb, NbN, and TaN thin-film bridges with and without geometrical nonuniformities in a magnetic field. Phys Rev B 2014;89:184511.
[100] Hu X, Holzwarth CW, Masciarelli D, Dauler EA, Berggren KK. Efficiently coupling light to superconducting nanowire single-photon detectors. IEEE Trans Appl Supercond 2009;19:336–40.
[101] Sprengers JP, Gaggero A, Sahin D, et al. Waveguide superconducting single-photon detectors for integrated quantum photonic circuits. Appl Phys Lett 2011;99:181110.
[102] Pernice WHP, Schuck C, Minaeva O, et al. High-speed and high-efficiency travelling wave single-photon detectors embedded in nanophotonic circuits. Nat Commun 2012;3:1325.
[103] Kovalyuk V, Hartmann W, Kahl O, et al. Absorption engineering of NbN nanowires deposited on silicon nitride nanophotonic circuits. Opt Express 2013;21:22683.
[104] Tyler NA, Barreto J, Villarreal-Garcia GE, et al. Modelling superconducting nanowire single photon detectors in a waveguide cavity. Opt Express 2016;24:8797.
[105] Kahl O, Ferrari S, Kovalyuk V, et al. Spectrally multiplexed single-photon detection with hybrid superconducting nanophotonic circuits. Optica 2017;4:557–62.
[106] Akhlaghi MK, Schelew E, Young JF. Waveguide integrated superconducting single-photon detectors implemented as near-perfect absorbers of coherent radiation. Nat Commun 2015;6:8233.
[107] Lita AE, Verma VB, Horansky RD, Shainline JM, Mirin RP, Nam S. Materials development for high efficiency superconducting nanowire single-photon detectors. MRS Proc 2015;1807:1–6.
[108] Yamashita T, Miki S, Qiu W, Fujiwara M, Sasaki M, Wang Z. Temperature dependent performances of superconducting nanowire single-photon detectors in an ultralow-temperature region. Appl Phys Express 2010;3:102502.
[109] Engel A, Inderbitzin K, Schilling A, et al. Temperature-dependence of detection efficiency in NbN and TaN SNSPD. IEEE Trans Appl Supercond 2013;23:2300505.
[110] Marsili F, Bitauld D, Fiore A, et al. High efficiency NbN nanowire superconducting single photon detectors fabricated on MgO substrates from a low temperature process. Opt Express 2008;16:3191–6.
[111] Kahl O, Ferrari S, Kovalyuk V, Goltsman GN, Korneev A, Pernice WHP. Waveguide integrated superconducting single-photon detectors with high internal quantum efficiency at telecom wavelengths. Sci Rep 2015;5:10941.
[112] Marsili F, Bellei F, Najafi F, et al. Efficient single photon detection from 500 nm to 5 μm wavelength. Nano Lett 2012;12:4799–804.
[113] Charaev I, Semenov A, Doerner S, Gomard G, Ilin K, Siegel M. Current dependence of the hot-spot response spectrum

of superconducting single-photon detectors with different layouts. Supercond Sci Technol 2017;30:025016.
[114] Polyakov SV. Single-photon detector calibration. In: Migdall A, Polyakov S, Fan J, Bienfang J, eds. Single-Photon Generation and Detection, Vol. 45. New York, USA, Academic Press, 2015, 1–16.
[115] Rath P, Vetter A, Kovalyuk V, et al. Travelling-wave single-photon detectors integrated with diamond photonic circuits – operation at visible and telecom wavelengths with a timing jitter down to 23 ps. in Proc. SPIE 9750, Integrated Optics: Devices, Materials, and Technologies 2016;XX:97500T.
[116] Vayshenker I, Li X, Livigni DJ, Scott TR, Cromer CL. Optical fiber power meter calibrations at NIST. Special Publication (NIST SP) – 250-54. 2000. https://doi.org/10.6028/nist.sp.250-54.
[117] López M, Hofer H, Kück S. Detection efficiency calibration of single-photon silicon avalanche photodiodes traceable using double attenuator technique. J Mod Opt 2015;62:1732–8.
[118] Ware M, Migdall A. Single-photon detector characterization using correlated photons: the march from feasibility to metrology. J Mod Opt 2004;51:1549–57.
[119] Polyakov SV, Migdall AL. High accuracy verification of a correlated-photon-based method for determining photon-counting detection efficiency. Opt Express 2007;15:1390–407.
[120] Müller I, Klein RM, Werner L. Traceable calibration of a fibre-coupled superconducting nano-wire single photon detector using characterized synchrotron radiation. Metrologia 2014;51:S329.
[121] Yamashita T, Miki S, Makise K, et al. Origin of intrinsic dark count in superconducting nanowire single-photon detectors. Appl Phys Lett 2011;99:161105.
[122] Shibata H, Fukao K, Kirigane N, Karimoto S, Yamamoto H. SNSPD With ultimate low system dark count rate using various cold filters. IEEE Trans Appl Supercond 2017;27:1–4.
[123] Cahall C, Gauthier DJ, Kim J. Scalable cryogenic readout circuit for a superconducting nanowire single-photon detector system. Rev Sci Instrum 2018;89:063117.
[124] Chunnilall CJ, Degiovanni IP, Kück S, Müller I, Sinclair AG. Metrology of single-photon sources and detectors: a review. Opt Eng 2014;53:081910.
[125] Fujiwara M, Tanaka A, Takahashi S, et al. Afterpulse-like phenomenon of superconducting single photon detector in high speed quantum key distribution system. Opt Express 2011;19:19562–71.
[126] Burenkov V, Xu H, Qi B, Hadfield RH, Lo H-K. Investigations of afterpulsing and detection efficiency recovery in superconducting nanowire single-photon detectors. J Appl Phys 2013;113:213102.
[127] Marsili F, Najafi F, Dauler E, et al. Single-photon detectors based on ultranarrow superconducting nanowires. Nano Lett 2011;11:2048–53.
[128] Wayne MA, Bienfang JC, Polyakov SV. Simple autocorrelation method for thoroughly characterizing single-photon detectors. Opt Express 2017;25:20352–62.
[129] You L, Yang X, He Y, et al. Jitter analysis of a superconducting nanowire single photon detector. AIP Adv 2013;3:072135.
[130] Caloz M, Perrenoud M, Autebert C, et al. High-detection efficiency and low-timing jitter with amorphous superconducting nanowire single-photon detectors. Appl Phys Lett 2018;112:061103.
[131] Calandri N, Zhao Q-Y, Zhu D, Dane A, Berggren KK. Superconducting nanowire detector jitter limited by detector geometry. Appl Phys Lett 2016;109:152601.
[132] Wollman EE, Verma VB, Beyer AD, et al. UV superconducting nanowire single-photon detectors with high efficiency, low noise, and 4 K operating temperature. Opt Express 2017;25:26792–801.
[133] Zhu D, Choi H, Lu T-J, et al. Superconducting nanowire single-photon detector on aluminum nitride. in Conference on Lasers and Electro-Optics 2016:paper FTu4C.1.
[134] Taillaert D, Van Laere F, Ayre M, et al. Grating couplers for coupling between optical fibers and nanophotonic waveguides. Jpn J Appl Phys 2006;45:6071.
[135] Divochiy A, Marsili F, Bitauld D, et al. Superconducting nanowire photon-number-resolving detector at telecommunication wavelengths. Nat Photonics 2008;2:302–6.
[136] Jahanmirinejad S, Frucci G, Mattioli F, et al. Photon-number resolving detector based on a series array of superconducting nanowires. Appl Phys Lett 2012;101:072602.
[137] Sahin D, Gaggero A, Zhou Z, et al. Waveguide photon-number-resolving detectors for quantum photonic integrated circuits. Appl Phys Lett 2013;103:111116.
[138] Lusardi N, Los JWN, Gourgues RBM, Bulgarini G, Geraci A. Photon counting with photon number resolution through superconducting nanowires coupled to a multi-channel TDC in FPGA. Rev Sci Instrum 2017;88:035003.
[139] Zhu D, Zhao Q-Y, Choi H, et al. A scalable multi-photon coincidence detector based on superconducting nanowires. Nat Nanotechnol 2018;13:596–601.
[140] Renema JJ, Frucci G, Zhou Z, et al. Modified detector tomography technique applied to a superconducting multiphoton nanodetector. Opt Express 2012;20:2806–13.
[141] Elezov MS, Semenov AV, An PP, et al. Investigating the detection regimes of a superconducting single-photon detector. J Opt Technol 2013;80:435.
[142] Ferrari S, Kahl O, Kovalyuk V, Goltsman GN, Korneev A, Pernice WHP. Waveguide-integrated single- and multi-photon detection at telecom wavelengths using superconducting nanowires. Appl Phys Lett 2015;106:151101.
[143] Feito A, Lundeen JS, Coldenstrodt-Ronge H, Eisert J, Plenio MB, Walmsley IA. Measuring measurement: theory and practice. New J Phys 2009;11:093038.
[144] Lundeen JS, Feito A, Coldenstrodt-Ronge H, et al. Tomography of quantum detectors. Nat Phys 2009;5:27–30.
[145] Akhlaghi MK, Majedi AH, Lundeen JS. Nonlinearity in single photon detection: modeling and quantum tomography. Opt Express 2011;19:21305–12.
[146] Natarajan CM, Zhang L, Coldenstrodt-Ronge H, et al. Quantum detector tomography of a time-multiplexed superconducting nanowire single-photon detector at telecom wavelengths. Opt Express 2013;21:893–902.
[147] Schuck C, Pernice WHP, Minaeva O, et al. Matrix of integrated superconducting single-photon detectors with high timing resolution. IEEE Trans Appl Supercond 2013;23:2201007.
[148] Buckley S, Chiles J, McCaughan AN, et al. All-silicon light-emitting diodes waveguide-integrated with superconducting single-photon detectors. Appl Phys Lett 2017;111:141101.
[149] Schuck C, Guo X, Fan L, Ma X, Poot M, Tang HX. Quantum interference in heterogeneous superconducting-photonic

circuits on a silicon chip – supplementary note 2. Nat Commun 2016;7:10352.
[150] Lamas-Linares A, Calkins B, Tomlin NA, et al. Nanosecond-scale timing jitter for single photon detection in transition edge sensors. Appl Phys Lett 2013;102:231117.
[151] Martinez NJD, Gehl M, Derose CT, et al. Single photon detection in a waveguide-coupled Ge-on-Si lateral avalanche photodiode. Opt Express 2017;25:16130–9.
[152] Becker W. The bh TCSPC Handbook, 7th ed. Becker&Hickl GmbH, 2017.
[153] Schuck C, Pernice WHP, Tang HX. Waveguide integrated low noise NbTiN nanowire single-photon detectors with milli-Hz dark count rate. Sci Rep 2013;3:1893.
[154] Calkins B, Mennea PL, Lita AE, et al. High quantum-efficiency photon-number-resolving detector for photonic on-chip information processing. Opt Express 2013;21:22657–70.
[155] Vetter A, Ferrari S, Patrik Rath P, et al. Cavity-enhanced and ultrafast superconducting single-photon detectors. Nano Lett 2016;16:7085–92.
[156] quTAG, qutools, 27-Jan-2016. [Online]. Available: https://www.qutools.com/qutag/. [Accessed: 13-Jul-2018].
[157] Münzberg J, Vetter A, Beutel F, et al. Superconducting nanowire single-photon detector implemented in a 2D photonic crystal cavity. Optica 2018;5:658–65.
[158] Najafi F, Mower J, Harris NC, et al. On-chip detection of non-classical light by scalable integration of single-photon detectors. Nat Commun 2015;6:5873.
[159] Li J, Kirkwood RA, Baker LJ, et al. Nano-optical single-photon response mapping of waveguide integrated molybdenum silicide (MoSi) superconducting nanowires. Opt Express 2016;24:13931–8.
[160] Khasminskaya S, Pyatkov F, Słowik K, et al. Fully integrated quantum photonic circuit with an electrically driven light source. Nat Photonics 2016;10:727–32.
[161] Cavalier P, Villégier J-C, Feautrier P, Constancias C, Morand A. Light interference detection on-chip by integrated SNSPD counters. AIP Adv 2011;1:042120.
[162] Guo X, Zou C, Schuck C, Jung H, Cheng R, Tang HX. Parametric down-conversion photon-pair source on a nanophotonic chip. Light Sci Appl 2017;6:e16249.
[163] Schuck C, Pernice WHP, Tang HX. NbTiN superconducting nanowire detectors for visible and telecom wavelengths single photon counting on Si3N4 photonic circuits. Appl Phys Lett 2013;102:051101.
[164] Beyer AD, Briggs RM, Marsili F, et al. Waveguide-coupled superconducting nanowire single-photon detectors, in 2015 Conference on Lasers and Electro-Optics (CLEO), 2015, 1–2.
[165] Shainline JM, Buckley SM, Nader N, et al. Room-temperature-deposited dielectrics and superconductors for integrated photonics. Opt Express 2017;25:10322–34.
[166] Reithmaier G, Kaniber M, Flassig F, et al. On-chip generation, routing, and detection of resonance fluorescence. Nano Lett 2015;15:5208–13.
[167] Digeronimo GE, Petruzzella M, Birindelli S, et al. Integration of single-photon sources and detectors on GaAs. Photonics 2016;3:55.
[168] Kaniber M, Flassig F, Reithmaier G, Gross R, Finley JJ. Integrated superconducting detectors on semiconductors for quantum optics applications. Appl Phys B 2016;122:115.
[169] Tanner MG, Alvarez LSE, Jiang W, Warburton RJ, Barber ZH, Hadfield RH. A superconducting nanowire single photon detector on lithium niobate. Nanotechnology 2012;23:505201.
[170] Höpker JP, Bartnick M, Meyer-Scott E, et al. Towards integrated superconducting detectors on lithium niobate waveguides. in Quantum Photonic Devices 2017;10358:1035809.
[171] Kahl O, Ferrari S, Rath P, Vetter A, Nebel C, Pernice WHP, High efficiency on-chip single-photon detection for diamond nanophotonic circuits. J Light Technol 2016;34:249–55.
[172] Rath P, Kahl O, Ferrari S, et al. Superconducting single-photon detectors integrated with diamond nanophotonic circuits. Light Sci Appl 2015;4:e338.
[173] Atikian HA, Meesala S, Burek MJ, et al. Novel fabrication of diamond nanophotonics coupled to single-photon detectors. SPIE Newsroom. 2017.
[174] Bogdanov S, Shalaginov MY, Boltasseva A, Shalaev VM. Material platforms for integrated quantum photonics. Opt Mater Express 2017;7:111–32.
[175] Suzuki N. FDTD analysis of two-photon absorption and free-carrier absorption in Si high-index-contrast waveguides. J Light Technol 2007;25:2495–501.
[176] Xiao S, Khan MH, Shen H, Qi M. Two-photon absorption induced thermal-optic effect in high-q silicon microring resonators. in LEOS 2007 – IEEE Lasers and Electro-Optics Society Annual Meeting Conference Proceedings, 2007, 890–891.
[177] Abdollahi S, Moravvej-Farshi MK. Effects of heat induced by two-photon absorption and free-carrier absorption in silicon-on-insulator nanowaveguides operating as all-optical wavelength converters. Appl Opt 2009;48:2505–14.
[178] Słysz W, Guziewicz M, Borysiewicz MA, et al. Ultrathin NbN films for superconducting single-photon detectors. Acta Phys Pol A 2011;120:200–3.
[179] Temple-Boyer P, Rossi C, Saint-Etienne E, Scheid E. Residual stress in low pressure chemical vapor deposition SiNx films deposited from silane and ammonia. J Vac Sci Technol Vac Surf Films 1998;16:2003–7.
[180] Bauters JF, Heck MJR, John D, et al. Ultra-low-loss high-aspect-ratio Si_3N_4 waveguides. Opt Express 2011;19:3163–74.
[181] Poot M, Schuck C, Ma X, Guo X, Tang HX. Design and characterization of integrated components for SiN photonic quantum circuits. Opt Express 2016;24:6843–60.
[182] Roeloffzen CGH, Zhuang L, Taddei C, et al. Silicon nitride microwave photonic circuits. Opt Express 2013;21:22937–61.
[183] Ovvyan AP, Gruhler N, Ferrari S, Pernice WHP. Cascaded Mach-Zehnder interferometer tunable filters. J Opt 2016;18:064011.
[184] Elshaari AW, Zadeh IE, Jöns KD, Zwiller V. Thermo-optic characterization of silicon nitride resonators for cryogenic photonic circuits. IEEE Photonics J 2016;8:1–9.
[185] Thyrrestrup H, Kiršanskė G, Jeannic HL, et al. Quantum optics with near-lifetime-limited quantum-dot transitions in a nanophotonic waveguide. Nano Lett 2018;18:1801–6.
[186] Oda H, Yamanaka A, Ozaki N, Ikeda N, Sugimoto Y. Operation of an InAs quantum-dot embedded GaAs photonic crystal slab waveguide laser by using two-photon pumping for photonics integrated circuits. AIP Adv 2016;6:065215.
[187] Davanco M, Liu J, Sapienza L, et al. Heterogeneous integration for on-chip quantum photonic circuits with single quantum dot devices. Nat Commun 2017;8:889.

[188] Midolo L, Hansen SL, Zhang W, et al. Electro-optic routing of photons from a single quantum dot in photonic integrated circuits. Opt Express 2017;25:33514–26.
[189] Balram KC, Davanço M, Lim JY, Song JD, Srinivasan K. Moving boundary and photoelastic coupling in GaAs optomechanical resonators. Optica 2014;1:414–20.
[190] Xiong C, Pernice WHP, Sun X, Schuck C, Fong KY, Tang HX. Aluminum nitride as a new material for chip-scale optomechanics and nonlinear optics. New J Phys 2012;14:095014.
[191] Tadesse SA, Li M. Sub-optical wavelength acoustic wave modulation of integrated photonic resonators at microwave frequencies. Nat Commun 2014;5:5402.
[192] Xiong C, Pernice WHP, Tang HX. Low-Loss, Silicon integrated, aluminum nitride photonic circuits and their use for electro-optic signal processing. Nano Lett 2012;12:3562–8.
[193] Zhu S, Lo G-Q. Aluminum nitride electro-optic phase shifter for backend integration on silicon. Opt Express 2016;24:12501.
[194] Jung H, Tang HX. Aluminum nitride as nonlinear optical material for on-chip frequency comb generation and frequency conversion. Nanophotonics 2016;5:263–71.
[195] Bazzan M, Sada C. Optical waveguides in lithium niobate: recent developments and applications. Appl Phys Rev 2015;2:040603.
[196] Alibart O, D'Auria V, De Micheli M, et al. Quantum photonics at telecom wavelengths based on lithium niobate waveguides. J Opt 2016;18:104001.
[197] Bonneau D, Lobino M, Jiang P, et al. Fast path and polarization manipulation of telecom wavelength single photons in lithium niobate waveguide devices. Phys Rev Lett 2012;108:053601.
[198] Burek MJ, Cohen JD, Meenehan SM, et al. Diamond optomechanical crystals. Optica 2016;3:1404–11.
[199] Mitchell M, Khanaliloo B, Lake DP, Masuda T, Hadden JP, Barclay PE. Single-crystal diamond low-dissipation cavity optomechanics. Optica 2016;3:963–70.
[200] Rath P, Khasminskaya S, Nebel C, Wild C, Pernice WHP. Diamond-integrated optomechanical circuits. Nat Commun 2013;4:1690.
[201] Rath P, Ummethala S, Diewald S, et al. Diamond electro-optomechanical resonators integrated in nanophotonic circuits. Appl Phys Lett 2014;105:251102.
[202] Rath P, Hirtz M, Lewes-Malandrakis G, Brink D, Nebel C, Pernice WHP. Diamond nanophotonic circuits functionalized by dip-pen nanolithography. Adv Opt Mater 2015;3:328–35.
[203] Aharonovich I, Greentree AD, Prawer S. Diamond photonics. Nat Photonics 2011;5:397.
[204] Gruhler N, Yoshikawa T, Rath P, et al. Diamond on aluminum nitride as a platform for integrated photonic circuits. Phys Status Solidi A 2016;213:2075–80.
[205] Lindenmann N, Balthasar G, Hillerkuss D, et al. Photonic wire bonding: a novel concept for chip-scale interconnects. Opt Express 2012;20:17667–77.
[206] Semenov AD, Gol'tsman GN, Sobolewski R. Hot-electron effect in superconductors and its applications for radiation sensors. Supercond Sci Technol 2002;15:R1.
[207] Matthias BT, Geballe TH, Compton VB. Superconductivity. Rev Mod Phys 1963;35:1–22.
[208] Courtney TH, Reintjes J, Wulff J. Critical field measurements of superconducting niobium nitride. J Appl Phys 1965;36:660–1.
[209] Vachtomin YB, Finkel MI, Antipov SV, et al. Gain Bandwidth of photon-cooled HEB mixer made of NbN thin film with MgO buffer layer on Si. Int Symp Space Tetrahertz Technol Harv Univ Camb MA 26–28 May 2002, 2002, 259–70.
[210] Antonova EA, Dzhuraev DR, Motulevich GP, Sukhov VA. Superconducting energy gap of niobium nitride. Sov Phys – JETP 1981;53:1270–1.
[211] Hong T, Choi K, Sim KI, et al. Terahertz electrodynamics and superconducting energy gap of NbTiN. J Appl Phys 2013;114:243905.
[212] Choi HJ, Roundy D, Sun H, Cohen ML, Louie SG. The origin of the anomalous superconducting properties of MgB2. Nature 2002;418:758–60.
[213] Kes PH, Tsuei CC. Two-dimensional collective flux pinning, defects, and structural relaxation in amorphous superconducting films. Phys Rev B 1983;28:5126–39.
[214] Nagamatsu J, Nakagawa N, Muranaka T, Zenitani Y, Akimitsu J. Superconductivity at 39 K in magnesium diboride. Nature 2001;410:63.
[215] Klimov A, Słysz W. Guziewicz M, Kolkovsky V, Zaytseva I, Malinowski A. Characterization of the critical current and physical properties of superconducting epitaxial NbTiN sub-micron structures. Phys C Supercond Appl 2017;536:35–8.
[216] Velasco AE, Cunnane DP, Frasca S, et al. High-operating-temperature superconducting nanowire single photon detectors based on magnesium diboride. in 2017 Conference on Lasers and Electro-Optics (CLEO), 2017, 1–2.
[217] Kitaygorsky J, Komissarov I, Jukna A, et al. Dark counts in nanostructured NbN superconducting single-photon detectors and bridges. IEEE Trans Appl Supercond 2007;17:275–8.
[218] Zhang L, Peng W, You LX, Wang Z. Superconducting properties and chemical composition of NbTiN thin films with different thickness. Appl Phys Lett 2015;107:122603.
[219] Korneeva YP, Mikhailov MY, Pershin YP, et al. Superconducting single-photon detector made of MoSi film. Supercond Sci Technol 2014;27:095012.
[220] Shcherbatenko M, Tretyakov I, Lobanov Y, et al. Nonequilibrium interpretation of DC properties of NbN superconducting hot electron bolometers. Appl Phys Lett 2016;109:132602.
[221] Zhou Z, Frucci G, Mattioli F, et al. Ultrasensitive N-photon interferometric autocorrelator. Phys Rev Lett 2013;110:133605.
[222] Gaudio R, Op't Hoog KPM, Zhou Z, Sahin D, Fiore A. Inhomogeneous critical current in nanowire superconducting single-photon detectors. Appl Phys Lett 2014;105:222602.
[223] Dane AE, McCaughan AN, Zhu D, et al. Bias sputtered NbN and superconducting nanowire devices. Appl Phys Lett 2017;111:122601.
[224] Guziewicz M, Slysz W, Borysiewicz MA, et al. Technology of ultrathin NbN and NbTiN films for superconducting photodetectors. Acta Phys Pol Ser A 2011;120:81–15.
[225] Dorenbos SN, Reiger EM, Perinetti U, Zwiller V, Zijlstra T, Klapwijk TM. Low noise superconducting single photon detectors on silicon. Appl Phys Lett 2008;93:131101.
[226] Tanner MG, Natarajan CM, Pottapenjara VK, et al. Enhanced telecom wavelength single-photon detection with NbTiN superconducting nanowires on oxidized silicon. Appl Phys Lett 2010;96:221109.
[227] Miki S, Takeda M, Fujiwara M, Sasaki M, Otomo A, Wang Z. Superconducting NbTiN nanowire single photon detectors with low kinetic inductance. Appl Phys Express 2009;2:075002.

[228] Yang X, You L, Zhang L, et al. Comparison of superconducting nanowire single-photon detectors made of NbTiN and NbN thin films. IEEE Trans Appl Supercond 2018;28:1–6.
[229] Kotsubo V, Radebaugh R, Hendershott P, et al. Compact 2.2 K cooling system for superconducting nanowire single photon detectors. IEEE Trans Appl Supercond 2017;27:1–5.
[230] Gemmell NR, Hills M, Bradshaw T, et al. A miniaturized 4 K platform for superconducting infrared photon counting detectors. Supercond Sci Technol 2017;30:11LT01.
[231] Yariv A. Integrated optics, in 1972 International Electron Devices Meeting. 1972;18:14.
[232] Ritter R, Gruhler N, Pernice WHP, Kübler H, Pfau T, Löw R. Coupling thermal atomic vapor to an integrated ring resonator. New J Phys 2016;18:103031.
[233] Hu X, Dauler EA, Molnar RJ, Berggren KK. Superconducting nanowire single-photon detectors integrated with optical nano-antennae. Opt Express 2011;19:17–31.
[234] Chong YD, Ge L, Cao H, Stone AD. Coherent perfect absorbers: time-reversed lasers. Phys Rev Lett 2010;105:053901.
[235] Zhai Y, Becerra FE, Glebov BL, et al. Photon-number-resolved detection of photon-subtracted thermal light. Opt Lett 2013;38:2171–3.
[236] Becerra FE, Fan J, Migdall A. Photon number resolution enables quantum receiver for realistic coherent optical communications. Nat Photonics 2015;9:48.
[237] Gaidash A, Egorov V, Gleim A. Revealing beam-splitting attack in a quantum cryptography system with a photon-number-resolving detector. JOSA B 2016;33:1451–5.
[238] Gerrits T, Thomas-Peter N, Gates JC, et al. On-chip, photon-number-resolving, telecommunication-band detectors for scalable photonic information processing. Phys Rev A 2011;84:060301.
[239] Marsili F, Bitauld D, Fiore A, et al. Photon-number-resolution at telecom wavelength with superconducting nanowires, in Recent Optical and Photonic Technologies, InTech, 2010.
[240] Fitch MJ, Jacobs BC, Pittman TB, Franson JD. Photon-number resolution using time-multiplexed single-photon detectors. Phys Rev A 2003;68:043814.
[241] Hayes RR, Yap DD. GaAs spiral optical waveguides for delay-line applications. J Light Technol 1993;11:523–8.
[242] Selvin PR. The renaissance of fluorescence resonance energy transfer. Nat Struct Mol Biol 2000;7:730–4.
[243] Becker W. Fluorescence lifetime imaging – techniques and applications. J Microsc 2012;247:119–36.
[244] Michalet X, Siegmund OHW, Vallerga JV, Jelinsky P, Millaud JE, Weiss S. Detectors for single-molecule fluorescence imaging and spectroscopy. J Mod Opt 2007;54:239.
[245] Kovalyuk V, Ferrari S, Kahl O, et al. On-chip coherent detection with quantum limited sensitivity. Sci Rep 2017;7:4812.
[246] Smit MK, Dam CV. PHASAR-based WDM-devices: principles, design and applications. IEEE J Sel Top Quantum Electron 1996;2:236–50.
[247] Okamoto K. Fundamentals of optical waveguides. Academic press, 2006.
[248] Aharonovich I, Castelletto S, Simpson DA, Su C-H, Greentree AD, Prawer S. Diamond-based single-photon emitters. Rep Prog Phys 2011;74:076501.
[249] Jacobs SF. Optical heterodyne (coherent) detection. Am J Phys 1988;56:235–45.
[250] Lobanov Y, Shcherbatenko M, Shurakov A, et al. Heterodyne detection at near-infrared wavelengths with a superconducting NbN hot-electron bolometer mixer. Opt Lett 2014;39:1429.
[251] Jiang LA, Luu JX. Heterodyne detection with a weak local oscillator. Appl Opt 2008;47:1486–503.
[252] Hargart F, Kessler CA, Schwarzbäck T, et al. Electrically driven quantum dot single-photon source at 2 GHz excitation repetition rate with ultra-low emission time jitter. Appl Phys Lett 2013;102:011126.
[253] Lee JP, Murray E, Bennett AJ, et al. Electrically driven and electrically tunable quantum light sources. Appl Phys Lett 2017;110:071102.
[254] Finley JJ, Ashmore AD, Lemaître A, et al. Charged and neutral exciton complexes in individual self-assembled InGaAs quantum dots. Phys Rev B 2001;63:073307.
[255] Bardot C, Schwab M, Bayer M, Fafard S, Wasilewski Z, Hawrylak P. Exciton lifetime in inGaAs quantum dot molecules. Phys Rev B 2005;72:035314.
[256] Sahin D, Gaggero A, Hoang TB, et al. Integrated autocorrelator based on superconducting nanowires. Opt Express 2013;21:11162–70.
[257] Zhou Z, Yin B, Michel J. On-chip light sources for silicon photonics. Light Sci Appl 2015;4:e358.
[258] Elshaari AW, Zadeh IE, Fognini A, et al. On-chip single photon filtering and multiplexing in hybrid quantum photonic circuits. Nat Commun 2017;8:379.
[259] Vijayaraghavan A, Blatt S, Weissenberger D, et al. Ultra-large-scale directed assembly of single-walled carbon nanotube devices. Nano Lett 2007;7:1556–60.
[260] Bachilo SM, Strano MS, Kittrell C, Hauge RH, Smalley RE, Weisman RB. Structure-assigned optical spectra of single-walled carbon nanotubes. Science 2002;298:2361–6.
[261] Mori T, Yamauchi Y, Honda S, Maki H. An electrically driven, ultrahigh-speed, on-chip light emitter based on carbon nanotubes. Nano Lett 2014;14:3277–83.
[262] Thomay T, Polyakov SV, Gazzano O, et al. Simultaneous, full characterization of a single-photon state. Phys Rev X 2017;7:041036.
[263] Hong CK, Ou ZY, Mandel L. Measurement of subpicosecond time intervals between two photons by interference. Phys Rev Lett 1987;59:2044–6.
[264] Meany T, Biggerstaff DN, Broome MA, et al. Engineering integrated photonics for heralded quantum gates. Sci Rep 2016;6:25126.
[265] Peruzzo A, Laing A, Politi A, Rudolph T, O'Brien JL. Multimode quantum interference of photons in multiport integrated devices. Nat Commun 2011;2:224.
[266] Heeres RW, Dorenbos SN, Koene B, Solomon GS, Kouwenhoven LP, Zwiller V. On-chip single plasmon detection. Nano Lett 2010;10:661–4.
[267] Heeres RW, Kouwenhoven LP, Zwiller V. Quantum interference in plasmonic circuits. Nat Nanotechnol 2013;8:719–22.
[268] Shainline JM, Buckley SM, Mirin RP, Nam SW. Superconducting optoelectronic circuits for neuromorphic computing. Phys Rev Appl 2017;7:034013.
[269] Pereda AE. Electrical synapses and their functional interactions with chemical synapses. Nat Rev Neurosci 2014;15:250–63.
[270] Shen Y, Harris NC, Skirlo S, et al. Deep learning with coherent nanophotonic circuits. Nat Photonics 2017;11:441–6.

[271] Rumelhart DE, Hinton GE, Williams RJ. Learning representations by back-propagating errors. Nature 1986;323:533–6.
[272] Chiles J, Buckley S, Nader N, Nam SW, Mirin RP, Shainline JM. Multi-planar amorphous silicon photonics with compact interplanar couplers, cross talk mitigation, and low crossing loss. APL Photonics 2017;2:116101.
[273] Hebb DO, The organization of behavior: a neuropsychological theory. Oxford, England, Wiley, 1949.
[274] Gabbiani F, Cox SJ. Chapter 30 – Neuronal networks, in mathematics for neuroscientists (Second edition), San Diego, Academic Press, 2017, 489–527.
[275] Akihama Y, Kanamori Y, Hane K. Ultra-small silicon waveguide coupler switch using gap-variable mechanism. Opt Express 2011;19:23658–63.
[276] Huang Q, Wu Y, Ma K, et al. Low driving voltage band-filling-based III–V-on-silicon electroabsorption modulator. Appl Phys Lett 2016;108:141104.